FACULTY OF INFORMATION TECHNOLOGY AND ELECTRICAL ENGINEERING
DEGREE PROGRAMME IN ELECTRONICS AND COMMUNICATIONS ENGINEERING
DEGREE PROGRAMME IN WIRELESS COMMUNICATIONS ENGINEERING

MASTER'S THESIS

RADIO CHANNEL CHARACTERIZATION AND CHANNEL MODEL EVALUATION WITH MEASURED 29 GHZ DATA FOR 5G COMMUNICATIONS

Author	Belén González Lozano
Supervisor	Pekka Kyösti
Second Examiner	Risto Vuohtoniemi
Technical Advisor	Essi Suikkanen

June 2020

González Lozano B. (2020) Radio Channel Characterization and Channel Model Evaluation with Measured 29 GHz Data for 5G Communications. University of Oulu, Faculty of Information Technology and Electrical Engineering, Degree Programme in Wireless Communications Engineering. Master's Thesis, 92 p.

ABSTRACT

In this thesis, a radio channel measured at 29 GHz for 5G communications is analysed and a corresponding channel model is evaluated. For this purpose, we have studied two different scenarios, where the first one represents a macrocell environment and the second one a microcell environment. Both scenarios had the same fifteen user equipment antenna locations and their main difference is the location from its base station. Indeed, these two different propagation scenarios are assumed to be static during the whole measurement.

Once the scenarios have been described, the delay spread, azimuth spread and path loss parameters from all the different paths that are received at each user equipment antenna are estimated. In order to do that, it has been considered whether those paths were on Line-Of-Sight or Non-Line-Of-Sight condition. As little research has been done at this frequency band for this innovative application, it is important to analyse and validate of those results. For that purpose, a MATLAB program has been designed for the automatic validation of those results, and at the same time, information about the channel behaviour is provided. Furthermore, these two scenarios have been analysed by implementing Keysight's Geometric Channel Modeling Tool, where a reconstruction of the channel has been obtained.

Key words: Macrocell, Microcell, Line-Of-Sight, Non-Light-Of-Sight, Delay Spread, Azimuth Spread, Path Loss, Channel Impulse Response, MUltiple SIgnal Classification, Uniform Circular Arrays.

TABLE OF CONTENTS

FOREWORD

This thesis has been carried out as a partial requirement for the competition of my academic year at the Center for Wireless Communications (CWC), at the University of Oulu, Finland. By doing this I will complete my studies at the Master in Telecommunication Engineering, from Universidad Politécnica de Madrid, Spain, which allowed me to come to Oulu and finish my last academic year studies here.

I would like to take this opportunity to, firstly, thank Dr. Pekka Kyösti for his time, knowledge and all the valuable advice, comments and dedication he had on my work. I think I could not have had a better supervisor. I would also like to thank my second supervisor, Tech.Lic. Risto Vuohtoniemi, as his experience and advice were really well appreciated. In addition to this, I would like to acknowledge Dr. Wei Fan, Associate Professor in Radio Propagation and OTA testing at University of Aalborg, for all his time, help and collaboration in this project, as he did not only provided us all the data but he also provided us the Channel Estimation's code. My gratitude also goes to Dr. Essi Suikkanen, from Keysight GCM Tool, for all her good advice, time and dedication to me. And last but not least, I would like to thank Dr. Matti Isohookana not only for finding me this amazing topic but also for all his good advice and support.

I really do not have words to express how grateful I am to all of you and all your dedication. You all have always been there for helping me and you have always lent me a hand whenever I needed it. Thank you.

Finally, I also want to thank all my family and friends, as they have not stopped supporting me, even when I was 4300 kilometers away from home. At long last, I would also like to thank all the new people that joined me during this amazing year and made me feel at home. Thank you.

Oulu, June, 18 2020

Belén González Lozano

LIST OF ABBREVIATIONS AND SYMBOLS

ABG	Alpha-Beta-Gamma Model
AoA	Azimuth Angle Of Arrival
AoD	Azimuth Angle of Departure
APS	Angular Power Spectrum
ASA	Cluster-wise RMS Azimuth Spread of Arrival
ASD	Cluster-wise RMS Azimuth Spread of Departure
BS	Base station
CI	Close-In Free Space Reference Distance Model
DDDPS	Double Directional Delay Power Spectrum
DL	Downlink
DOA	Direction Of Arrival
DOD	Direction Of Departure
EoA	Elevation Angle of Arrival
EoD	Elevation Angle of Departure
EsA	Cluster-wise RMS Elevation Spread of Arrival
EsD	Cluster-wise RMS Elevation Spread of Departure
FDD	Frequency Division Duplex
GCM	Geometric Channel Modeling
GSCM	Geometry-based Stochastic Channel Model
IS-GSCM	Irregular-shaped GSCM
LOS	Line-Of-Sight
MIMO	Multiple-input multiple-output
MS	Mobile Station
MUSIC	MUltiple SIgnal Classification
NLOS	Non Line-Of-Sight
OS	Open Street model
PDF	Probability Distribution Function
PDP	Power Delay Profile
rms	root-mean-square
RS-GSCM	Regular-shaped GSCM
SC	Street Canyon model

TDD	Time Division Duplex
UCA	Uniform Circular Array
UE	User equipment
UL	Uplink
VNA	Vector Network Analyser
4G	Fourth Generation
5G	Fifth Generation

A	Amplitude
B_c	Coherence bandwidth
c	Speed of light
c_{tot}	Total number of clusters
d	Distance between antennas
d_1	Distance obtained from the map in metres
d_1'	Distance obtained from the map in centimetres
d_1''	Distance obtained from the map in centimetres
d_2	Distance obtained from the delay value
f_c	Carrier frequency
F_0	0^{st} complex Fourier coefficient
F_1	1^{st} complex Fourier coefficient
h	Height difference between BS and UE
i	UE location's number
k	Last path received at a UE location
L_{bf}	Free space loss
l	Cluster's index
n_1	Refraction index of the first material
n_2	Refraction index of the second material
P_m	Time-integrated power
P_T	Transmitted power
P_R	Received power
$p(\theta)$	Angular distribution of multipath power
PL	Path loss

$PL_{CI\,Uma}$	Path loss by the CI model in a macrocell environment
$PL_{CI\,Umi\,OS}$	Path loss by the CI model in a microcell environment, open street model
$S_{a_{Uma}}$	Angular of arrival in a macrocell environment
$S_{a_{Umi}}$	Angular of arrival in a microcell environment
S_d	rms delay spread
$S_{d_{Uma}}$	rms delay spread in a macrocell environment
$S_{d_{Umi}}$	rms delay spread in a microcell environment
S_ϕ	Azimuth spread
T_c	Coherence time
T_m	Mean delay
Ψ	Direction Of Arrival
Ω	Direction of Departure
σ	Standard deviation
τ	Delay
θ_1	Angle of incidence
θ_2	Angle of refraction
ϕ	Azimuth direction
Λ	Shape factor angular spread
cm	centimetre
dB	decibel
GHz	gigahertz
km	kilometre
m	metre
ns	nanoseconds
W	watt
º	degrees

1 INTRODUCTION

Due to the colossal growth of the data rate and so the spectrum congestion for mobile communications, a new communication network is needed, fifth generation (5G). This new communication network meets consumer data demands, provides high data rates, stable connections, lower latency, and larger capacity. As this new generation network transmits data more efficiently, if we compare 5G with its previous generation, fourth generation (4G), this new communication network has the potential to be 40 times faster and suffer shorter lag times than 4G [1]. The reason why 5G is important is because through this communication network, we will be able to create multiple technologies, gadgets, and applications that are not yet invented. For instance, one of the most famous applications for 5G are the autonomous cars, where timely decisions are needed to avoid incidents.

The purpose of our project is to be able to characterise and define the radio channel model in a way that we can achieve more insight to develop communications in a 5G frequency band. Radio channel is the transmission medium between the transmitter and receiver for a wireless communication. Furthermore, radio channel characterization is the definition of the different parameters which are concerned in the communication such as power, delay spread, azimuth spread, elevation angle, etc. By characterising the medium, we are then able to understand better the channel's behaviour, and this is the aim of this thesis. The reason why this is important and also needed, is because due to this 5G innovation, the frequency bands in which this communication network operates, which go from 3.5 GHz until 6 GHz, but also from 24 GHz until 100 GHz [2], have not been exploited as much as the previous generations ones. Indeed, these previous generations networks operate in lower bands, for example 4G's frequency band goes from 700 MHz up to 2.7 GHz [3]. In other words, in this project we aim to understand the channel behaviour in a 5G frequency band, particularly at 29 GHz.

In this study, we will be characterising and evaluating a radio channel model for 5G communications. Firstly, we will implement the MUltiple SIgnal Classification (MUSIC) algorithm to estimate the Direction Of Arrival, DOA. This implementation is done by Professor Wei Fan from Alborg's University, and with it we can process the raw measured data in a way that we get information of the propagation channel, such as the number of paths and its elevation, azimuth, delay and amplitude values. Once we know those parameters, we will

implement a system that will automatically analyse those results with a MATLAB code. This will provide us information related to the delay and azimuth spread and so to the path loss, in a way that we can characterise the radio channel. With this MATLAB code we will also be able to compare how the values we have obtained differ from the reference ones. In this way, with this MATLAB code we will be able to check the validity of the delay spread, azimuth spread and path loss values, not only for our frequency band but also for any 5G high frequency band (24 GHz - 100 GHz). Furthermore, this code can also be used with either a macrocell or a microcell environment, and either Line-Of-Sight or Non Line-Of-Sight conditions. Afterwards, we will use Keysight Geometric Channel Modeling (GCM) Software Tool to compare and validate of the results obtained from the channel measurement, and to reconstruct the obtained channel. At the end, it is expected to know properly how do the parameters from the radio channel model behave at our frequency band, 29 GHz.

This thesis is organised as follows. First in Chapter 2 there is a background theory related to the radio channel models. Secondly in Chapter 3 it is detailed explained the scenario under evaluation, with a description of all the elements concerned. In Chapter 4 the results obtained from creating an analytic method with MATLAB are analysed while in Chapter 5, the values obtained from the previous chapter are checked out by using Keysight Geometric Channel Modeling Tool, and also the radio channel model is evaluated. The conclusion is drawn in Chapter 6 and a summary of all our work is in Chapter 7. Appendices contain information related to the path's estimation values, MATLAB code, path estimation and parameter's values, and can be found at the end of the document.

2 RADIO CHANNEL CHARACTERISTICS

This work is for a geometry-based stochastic channel model, where there are several parameters such as the Power Delay Profile, Double Directional Delay Power Spectrum, Coherence Bandwidth, Coherence Time, or the Delay Spread, Azimuth Spread and Path Loss, that must be considered in this study so they are described in this chapter.

2.1 Geometry based Stochastic Channel Model

The geometry-based stochastic channel model (GSCM), is broadly used in Multiple-input multiple-output (MIMO) channel modelling and it can be classified based on the effective scatterers' distribution. In this way we can distinguish regular-shaped GSCMs (RS-GSCMs), and irregular-shaped GSCMs (IS-GSCMs) [4]. In the model under study, we will be analysing a RS-GSCM as it is the same model used in Keysight GCM software Tool.

Through this channel model we are able to create an arbitrary Double Directional Radio Channel Model, where different antenna configurations and element patterns can be used. Related to the channel parameters, they are determined stochastically based on the statistical distributions attained by statistical distributions delivered from channel measurement [5]. This means that we can separate propagation parameters and antennas in a way that we obtain the channel characteristics by applying geometrical principles, which is done by summing contributions of rays with specific input parameters. These input parameters are delay, power, angle-of-arrival and Angle Of Departure [6].

Due to the fact that this model can be used with different scenarios and each of them with different parameters, a three phases method can be followed. This method can be seen in Figure 1.

As it is seen in Figure 1, the first step consists of defining the propagation scenarios. In this point, the environment, the antenna's height or for instance the mobility, should be considered. Once we have done that, we should choose which parameters we want to be measured, and this is done in the step named Generic Model. Once the scenarios and the generic model are defined, we can proceed with the Campaign Planning. Here parameters such as the channel sounder setup, the measurement route or the link budget should be analysed. After that, channel measurements are carried out in a step named Channel Measurements, and these results are saved in a massive memory, this step is named Measurement Data [5].

Once the data are processed and stored, we can move on to the second phase which focusses on the analysis of the data. Firstly, and according to the required parameters, the analysis methods are carried out in a way that we can obtain the data post-processing/analysis. Through that and with some statistical analysis, the parameters from the Probability Distribution Function (PDF) can be finally known [5].

At long last, the last phase of the process sets up everything in a way that the simulation can be done. Firstly, through random number generators and filters, the parameters are obtained. With those parameters and with the array responses, which are arising from the antennas, the MIMO transfer matrix can be generated. The simulation can be finally run once we have the channel realisations, which are the impulse responses of our study [5].

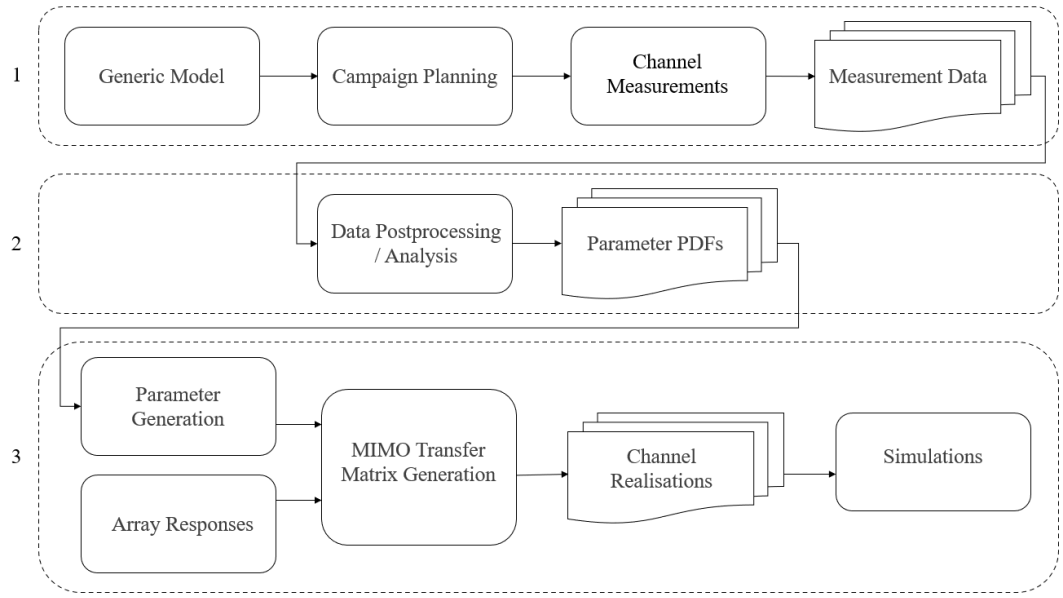

Figure 1. Channel modelling process.

2.2 Power Delay Profile

The Power Delay Profile (PDP), $P_h(\tau)$, can also be named as the multipath intensity profile, and is a function that represents the average power associated to a given multipath delay. A multipath propagation is a phenomenon in which the signals arrive at the receiver antenna by two or more propagation paths. As the PDP can be easily empirically measured [7], through this study it is estimated from measurements and modelled as discrete functions. In other words, for this analysis, the PDP has been calculated for each antenna location as the sum of all the paths from a certain delay bin.

2.3 Delay Spread

Delay Spread helps us to better understand how the transmitted signal has been either reflected or diffracted during its propagation link. In this way, an extreme delay time spread would give us the total time interval during which reflections with significant energy arrive [8].

The rms, root-mean-square, delay spread, S_d, highlights why under some specific circumstances, it is the only relevant parameter as the PDP of the channel does not have a significant influence. However, it should be also mentioned that S_d does not attain finite values for all physically reasonable signals [9].

The rms delay spread is defined as, [9]

$$\mathrm{S_d} = \sqrt{\frac{\int_{-\infty}^{\infty} \mathrm{P_h}(\tau)\, \tau^2\, \mathrm{d}\tau}{\mathrm{P_m}} - \mathrm{T_m^2}}\ , \tag{1}$$

where P_m represents the time-integrated power and it is defined as, [9]

$$\mathrm{P_m} = \int_{-\infty}^{\infty} \mathrm{P_h}(\tau)\, \mathrm{d}\tau\,, \tag{2}$$

and T_m represents the mean delay and it is defined as, [9]

$$\mathrm{T_m} = \frac{\int_{-\infty}^{\infty} \mathrm{P_h}(\tau)\, \tau\, \mathrm{d}\tau}{\mathrm{P_m}}\,. \tag{3}$$

2.4 Coherence Bandwidth and Coherence Time

The coherence bandwidth, B_c, is the bandwidth over which the channel transfer function remains virtually constant in a frequency domain, while the coherence time, T_c, represents the same concept as B_c but in the time domain [10].

It should be noticed the strong relationship between the coherence bandwidth and the delay spread, as they are inversely proportional, as seen in the next equation, [7]:

$$B_c = \frac{1}{S_d} . \quad (4)$$

2.5 Double Directional Delay Power Spectrum

Double Directional Delay Power Spectrum (DDDPS) depends only, as it can be seen from equation (5), on the Direction of Departure (DOD) Ω, Direction Of Arrival (DOA) Ψ, and delay τ, [9]:

$$\mathrm{DDDPS}(\Omega, \Psi, \tau) = \int \mathrm{P_s}(\Psi, \Omega, \tau, \mathrm{v})\mathrm{dv} . \quad (5)$$

In case marginal power distributions were independent, DDDPS could be defined by only three functions, where at the same time each of those functions depends on a different parameter, as seen in the following equation [9]:

$$\mathrm{DDDPS}(\Omega, \Psi, \tau) = \mathrm{APS}^{\mathrm{BaseStation}}(\Omega)\, \mathrm{APS}^{\mathrm{MobileStation}}(\Psi)\, \mathrm{P_h}(\tau) , \quad (6)$$

where APS is the Angular Power Spectrum. As it can be noticed, the APS at the Base Station (BS), and so the APS at the Mobile Station (MS) are independent of delay. Additionally, the APS at the BS is also independent of the direction in which the MS transmits and vice versa [9]. However, as this assumption is not always valid in reality, a more general model which assumes that the DDDPS consists of several clusters, c_{tot}, each of them with a separable DDDPS (where *l* stands for the cluster's index) is needed [9]:

$$\mathrm{DDDPS}(\Omega, \Psi, \tau) = \sum_{\mathrm{l}} \mathrm{P_l^{c_{tot}}}\, \mathrm{APS_l^{c_{tot},BS}}(\Omega)\, \mathrm{APS_l^{c_{tot},MS}}(\Psi)\, \mathrm{P_{h,l}^{c_{tot}}}(\tau) . \quad (7)$$

2.6 Azimuth Spread

Azimuth Spread is the azimuthal or angular direction, ϕ, from which the signal arrives at the receiver antenna.

When all the multi path components are incident in the horizontal plane, the azimuth spread is the second central moment of the APS.

The azimuth spread, S_ϕ, can be then calculated as seen in the next equation [9]:

$$S_\phi = \sqrt{\frac{\int \left|\exp(j\phi) - \mu_\phi\right|^2 APS(\phi) d\phi}{\int APS(\phi) d\phi}}, \quad (8)$$

where μ_ϕ is:

$$\mu_\phi = \frac{\int \exp(j\phi)\, APS(\phi) d\phi}{\int APS(\phi) d\phi}. \quad (9)$$

Both, delay spread and azimuth spread, are just a partial description of angular dispersion [9].

2.7 Path Loss

Path Loss is the attenuation due to the propagation effects between transmitter and receiver [9]. In other words, it is the ratio of transmitted and received power when antenna gains are removed. This parameter depends not only on the frequency range but also on the distance and some additional external parameters such as building height or the type of the environment. Due to that last factor, we can find multiple path loss models, such as for example for rural environments, suburban, urban, indoors, etc.

In general, it is considered as a deterministic parameter and it is usually defined as seen in the next equation, [11]:

$$\frac{P_R}{P_T} = G_T G_R \frac{1}{PL}, \quad (10)$$

where P_T represents the transmitted power (in W), P_R the received power (in W), G_T and G_R are the transmitter and receiver gain values respectively, and *PL* is the path loss. As we will see later in Section 4.1.3.3, if we are in Line-Of-Sight condition (LOS), path loss depends only on the distance, *d*, the carrier frequency, f_c, and the speed of light, *c*, as seen in the next equation, equation (11), [11]:

$$PL = \left(\frac{4\,\pi\,f_c\,d}{c}\right)^2 . \tag{11}$$

If we clear equation (10), we can then obtain the next one, equation (12), which shows exactly the relationship between the path loss and these parameters:

$$PL = G_T G_R \frac{P_T}{P_R} . \tag{12}$$

The next image helps us to better visualize this concept:

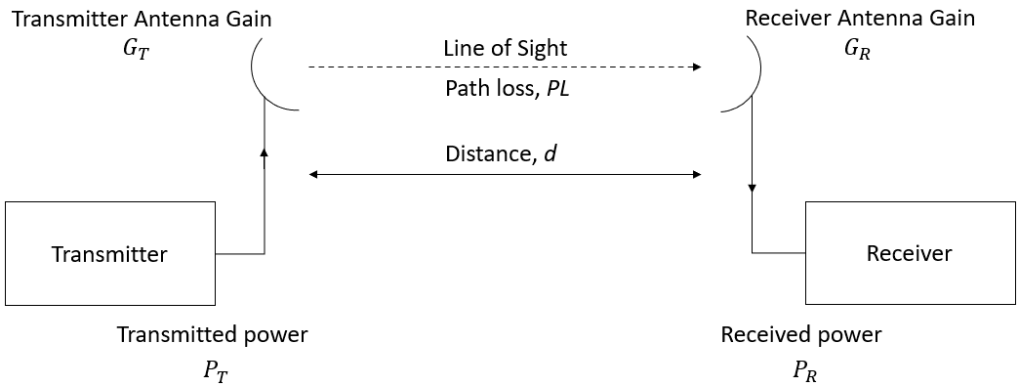

Figure 2. Path loss scheme.

In our study, due to the parameters we had, the overall path loss at each location was calculated by summing up all the received powers from the paths which satisfied the threshold limit for each UE location (this is explained in Section 4.1.1).

3 MEASUREMENT SCENARIO

The radio channel data was measured by University of Aalborg. These data sets contain an outdoor environment at a carrier frequency of 29 GHz, 2 GHz of bandwidth and 2000 frequency samples. In the following sections we will describe the two cases under study and its measurement set up as well.

3.1 Measurement cases

Firstly, we are going to describe the scenario and its different measurement cases. In this way, it is important to mention the presence of two receiver locations imitating base stations, where one was placed on the roof (indicated as 'Tx 1' in Figure 3) and the other one on the rod (indicated as 'Tx 2' in Figure 3), and fifteen transmitter locations imitating user equipment (UE) devices, or MS, denoted with red markers, see Figure 3. As it can be seen from that same figure, each UE had a different location along a trajectory. However, these trajectories were not measured neither simultaneously nor continuously (see Figure 4 and Figure 5). Along these lines, we will analyse two different cases. The first one concerns the scenario where the BS is placed on the roof, which represents a macrocell environment, as the BS is well above the roof top level which allows it to see further places and make larger cells, in other words, this improves the BS's coverage area. The second scenario is the one where the BS is placed on the rod, which represents a microcell environment, as the BS is placed below the roof top level and due to this its coverage area is smaller as the signal is more affected by obstructions.

Hereunder are some photos of the scenario. The first photo, Figure 3, shows the different BS's locations on the map marked with yellow circles. We would like to mention that by doing this work, we have realised that the second BS's position was not in the original placed marked with a yellow cross but in the one marked with a yellow circle. We became aware of this by looking at the LOS delay values, as the ones we had were smaller than what they should be if the BS did were in the cross mark. Despite this and as we have just mentioned, both scenarios had 15 possible UE locations, and the distance between two proximate array antenna locations was 1.5 m (see Figure 4 and Figure 5).

Figure 3. Top-view photo of the outdoor area with the BS locations shown in yellow.

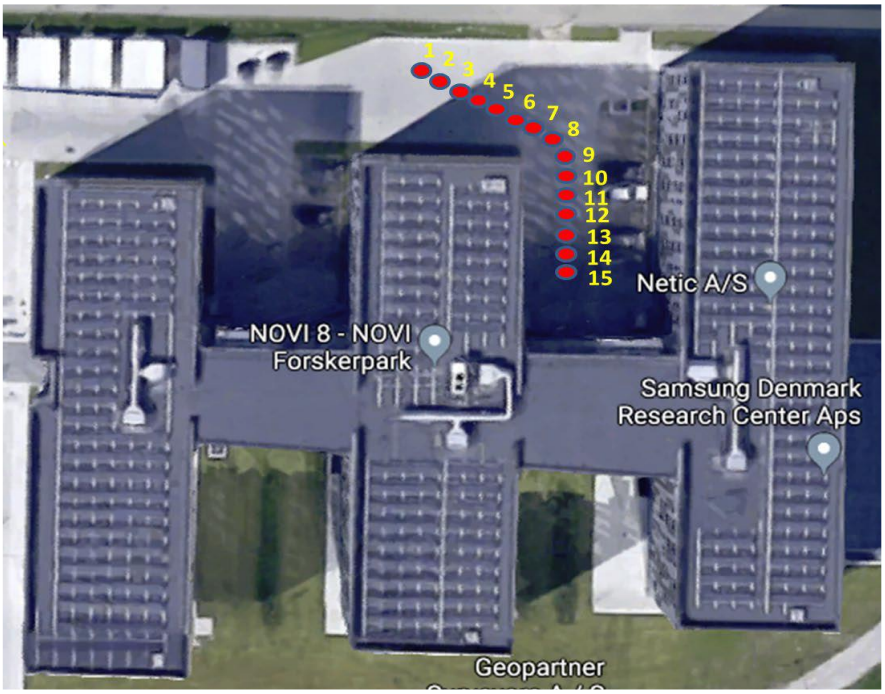

Figure 4. Top-view photo of the outdoor area with UE measurement points marked in red.

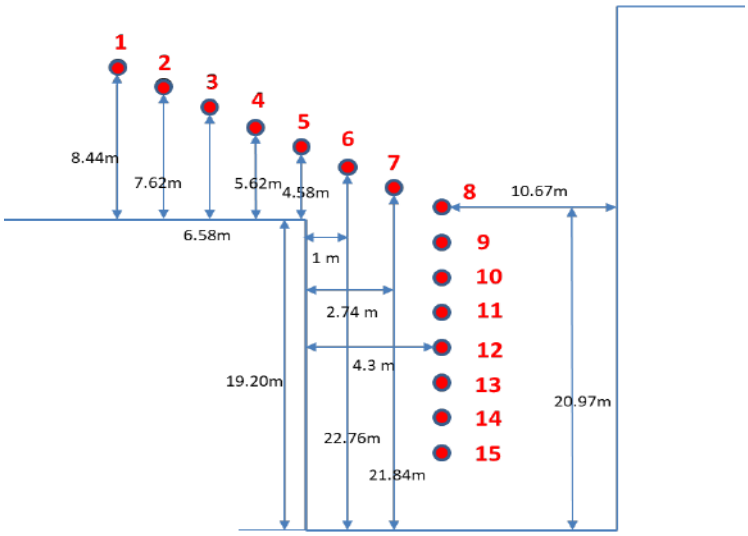

Figure 5. Top-view sketch of the outdoor area with UE measurement points marked.

Through the following figures, we aim to describe the materials of the surfaces that affect the propagation path. To begin with the first one, Figure 7 shows the location of the BS when it is placed on the roof. We can notice the presence of some metallic bicycle shelters, and if we look at Figure 3 and Figure 4, we can see that some of these bicycle shelters are quite close to the UE locations so they may obstruct the signal in a way that it is reflected. Despite the ground in this case is mainly asphalt, if we look at Figure 8 we can see that when the BS is placed on the rod, the ground is mainly a grass area. In this case, another dominant material as it can be seen, are the car's surfaces.

Figure 6. View of the first transmitter position (BS on the roof).

Figure 7. View from the second transmitter position (BS on the rod).

Indeed, both cases under study are affected by the building's surface. From Figure 8 we can see that the facade named as 'Wall A', is mostly cover with bricks while 'Wall C' contains also some windows over it. Finally, Figure 9 shows the facade named as 'Wall B', and it can be seen that it contains plenty of windows and, at the same time, it is all covered with some metallic plate surfaces.

Figure 8. View of walls A and C.

Figure 9. View of wall B.

Once we have analysed the environment of our scenarios, we can conclude, as we already introduced at the beginning of this section, that the first case, which is the one that covers the scenario where the BS is placed on the roof, represents a macrocell environment as the BS's height is higher than any obstacle or building present in the surroundings. The main characteristics of this scenario can be seen in Table 1, where we can also find the distances, which consider the height of the BS, to some UEs locations.

Table 1: 1st case characteristics

1st case	
BS's height	20 m
Building's height	4 levels
Distance to the 1st UE	50.85 m
Distance to the 8th UE	62.95 m

Nevertheless, the second case which concerns the scenario where the BS is placed on the rod, it represents a microcellular environment. In this way, as the BS's height is below the roof top level, it is expected to have more multipath components and also longer delays, as the paths travel through longer distances due to the reflections or double reflections caused by the obstacles, cars or buildings. The main characteristics of this scenario can be seen in the next table, Table 2.

Table 2: 2nd case characteristics

2nd case	
BS's height	3 m
Building's height	4 levels
Distance to the 1st UE	54.76 m
Distance to the 8th UE	47.26 m

3.2 Measurement set up

The aim of this section is to describe all the measurement devices used in this study. In practice, many spatial positions along the horizontal circle were measured in each UE location. As we have already mentioned, the measurement data is a collection of wide band frequency responses from two BSs to fifteen UE locations and 360 virtual antenna positions within each location, as explained in Section 3.2.1.

3.2.1 Measurement equipment

To begin with, we would like to mention that the measurement device was a vector network analyser (VNA) connected through optical cable. In this study, the BS antenna was a single horn with wide beam width, and the UE locations were measured with a Uniform Circular Array (UCA). All the numerical measurement parameters and all the measurement settings can be found in Table 3.

Table 3: Numerical measurement parameters and measurement settings

		1st case "Roof"	2nd case "Rod"
BS locations	Type of antenna	Horn antenna	Horn antenna
	Antenna's boresight direction in azimuth	15º	Direction of radiation towards the UE positions
	Antenna's boresight direction in elevation	25º	
	Antenna's height	20 m, the antenna is placed on the roof	3 m, the antenna is placed on the rod
	Photo of the antenna	See Figure 10	See Figure 11
UE locations	Type of antenna	Homemade vertically polarized biconical antenna	Homemade vertically polarized biconical antenna
	Number of elements	360	360
	Radius (m)	0.25	0.25
	Antenna's height (m)	1	1
	Number of antennas positions	15	15
	Description of the azimuth	0º points to the East and it travels through the array clockwise	0º points to the East and it travels through the array clockwise
	Description of the elevation	0º is up 90º is the horizon 180º is down	0º is up 90º is the horizon 180º is down
Carrier frequency		29 GHz	
Bandwidth		2 GHz	
Frequency samples		2000	

Hereunder are some photos of the antennas used as a BS for each scenario. Figure 10 shows the antenna used as a BS for the 1st case while Figure 11 shows the antenna used as a BS for the 2nd case.

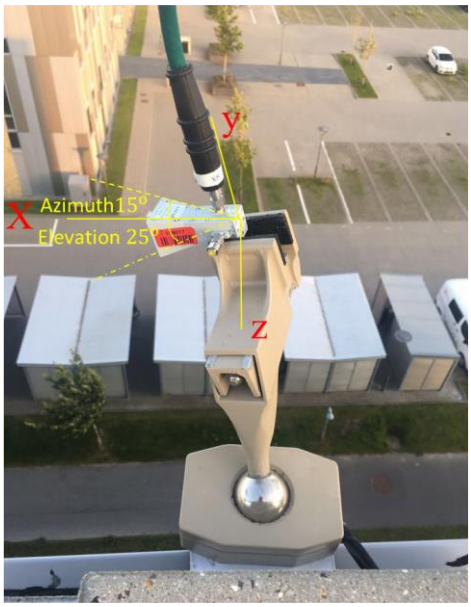

Figure 10. Photo of the 1st case horn antenna.

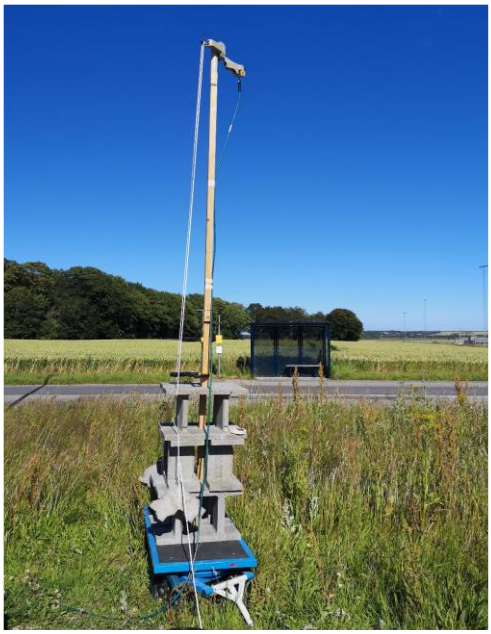

Figure 11. Photo of the 2nd case horn antenna.

Related to the UCAs, these are antenna systems that highlight due to its symmetry as they have the ability to scan a beam azimuthally through 360º with little change in neither the beam width nor the sidelobe level. This implies the possibility to examine the estimation of the direction of arrival from the incoming signals and beamforming [12]. Regarding the

beamforming, UCAs have great capabilities in directing the maximum towards the direction of the signal of interest and deep nulls towards the directions of the signals not of interest [12]. In Figure 12 there is a MATLAB representation from the UCA used in this study. As it can be seen, the UCA has 360 elements, all of them distributed in a circle of a 0.25 m radius, and its height is 1 m. Just as we have mentioned before in Table 3, for this project and based on the raw data measured system, we have considered that the azimuth's origin, 0º, is pointing to the East and it travels through the array clockwise. Concerning the elevation, in our study we have defined that 90º is pointing to the horizon, 0º is up and 180º is down.

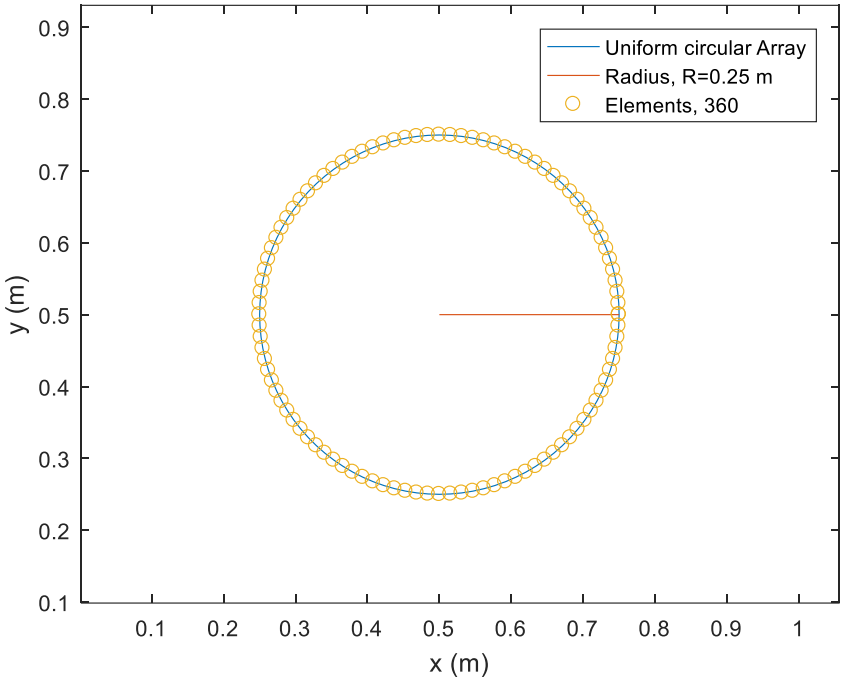

Figure 12. Uniform Circular Array scheme.

3.2.2 Channel estimation

Once we have described the antennas and elements used in this study, we are going to discuss the channel estimation method. The estimation of the direction-of-arrival (DOA), is approached by the MUltiple SIgnal Classification (MUSIC) algorithm. MUSIC is a subspace-based algorithm which provides high angle and delay estimation resolution [13]. This algorithm takes advantage of the orthogonality between the signal vectors and the noise subspace. In other words, MUSIC makes possible some element-space operations such as a reduced computation or the performance in correlated-source scenarios. The reduced computation is achieved by the

estimation of the subspace through real-valued eigen decompositions and the performance in correlated-source scenarios by the attendant forward-backward averaging effect [12].

In this section, we would like to highlight the importance of Professor Wei Fan's MATLAB code, which follows several steps. Through the first one, it applies MUSIC algorithm to obtain the angle delay estimation, and the estimated number of paths for each UE location, in other words, it finds the angles and delays of the different sources. After that, it estimates the PDP by applying beamforming and nulling operation for each path over the spatial domain. This is all done by only knowing the frequency and the channel response for each of the 360 elements and 2000 frequency samples of the UCA [13].

Once we have those results, we can then proceed to the representation of all the significant paths, and also with the calculation of the delay spread, azimuth spread and path loss values for each scenario. This is done by implementing our own MATLAB code, which can be found in Appendix 3. This MATLAB code also provides automatically the information needed to know whether the input parameters are reliable enough or not by comparing the results obtained with some reference values, as we will see later on Section 4.1.3.

4 RESULTS

To begin with, once we have processed the measured data as described in Section 3.2.2 and obtained path powers, delays, and angles, we are then going to characterise the massive MIMO radio channel communication by analysing some results such as the number and trajectory of paths, delay spread, azimuth spread and path loss. Once we have obtained that information with our own MATLAB code, we will then simulate the scenarios under study with Keysight GCM Software Tool so we can compare the results obtained with MATLAB and this software, reconstruct the channel, and draw conclusions.

4.1 MATLAB analysis

Through this section, we will firstly analyse the propagation path parameters calculated by Professor Wei Fan in order to define and characterise the environment and the paths' routes with our own MATLAB code. After that, we will then be able to calculate (through MATLAB) metrics such as delay spread, azimuth spread and path loss, from the estimated parameters.

4.1.1 Propagation parameters

In this subsection, we are going to analyse the multipath effects of the transmission. First of all, we analyse the origin of the paths as each of them arrive at the receiver with different delay, different azimuth, different elevation and different intensity level. In other words, this means that they arrive at the antenna through different propagation paths. The reason for this is the presence of obstacles (see Figure 3) that may obstruct and either reflect or diffract the signal. Based on this, in the following figures we can notice, for each array antenna location, how many paths arrived to them and its azimuth, elevation and delay values. The results from these parameters help us to determine where the paths come from.

Hereunder, we are going to analyse one UE location for the 1st case, the one in the third location which is in LOS with its BS, and three UE locations for the 2nd case. In this last case, the UE antennas that we have chosen are the ones in the locations number two and six, in LOS with its BS, and location number fourteen, in NLOS condition with its BS. The reason why we have chosen these locations is because through them, we can analyse all the possible results from the rest of the UE locations. We would also like to mention that within each figure, the

dots that can be seen have different colour coding regarding its received power magnitude level. Indeed, this magnitude represents the power profile in dB.

Starting with the 1st case, we can see from Figure 13, that for this antenna location we receive 5 different paths due to the propagation effect. As it can be seen, each of those paths arrived at the antenna with different intensity, different delay, different elevation, and different azimuth values. The first path that arrives at the antenna is the one shown in yellow as it is the one with the shortest delay (179.5 ns) and the highest power level (-76.3 dBm). This path, arrived at the antenna with an elevation of 81º and an azimuth of 200º. The reason why the elevation's value is high is not only because of the height of the antennas, as the BS antenna is at 22 m height and the transmitters are just at 1m height, but also because of the distance between them, which is around 53 m. The azimuth's value is totally reasonable with the definition of our study, as this UE location is in LOS with the BS and due to azimuth's reference definition, this value should be between 180º and 270º, and as we have already introduced, in this case the azimuth is 200º, which satisfies the previous condition. However, we would like to emphasize that the azimuth helps us to explain the paths' trajectory. For example if we look at the azimuth's value from the second path at this same UE location (147º), we can estimate that this path reaches the antenna by firstly reflecting on the building, at the wall named 'A' (see Figure 3). This is drawn further down in Figure 20.

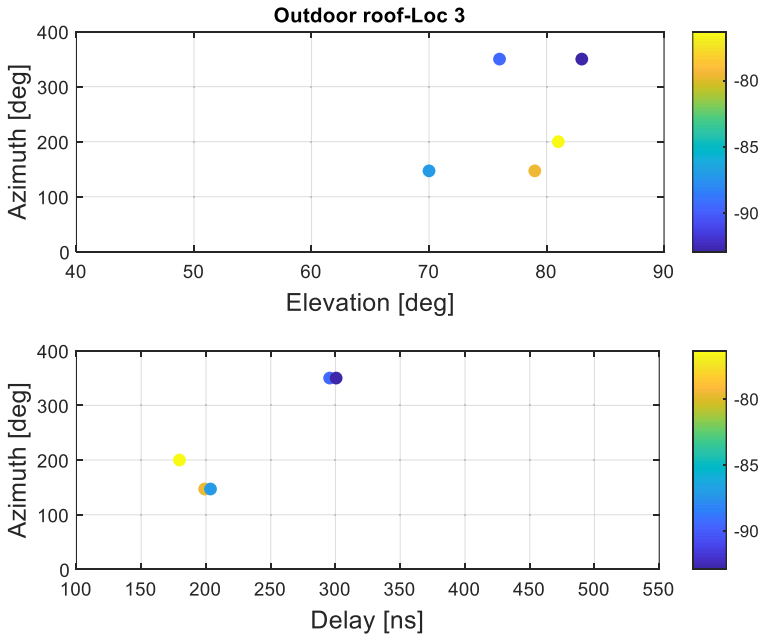

Figure 13. Multipath at the 3rd UE location in the 1st case.

If we now focus on the 2nd case, in Figure 14 we can see that 3 different paths are arriving at the sixth antenna location when the BS is placed on the rod. Due to the propagation effects, each of those paths arrived again with different intensity, delay, elevation, and azimuth values. The first path that arrived is again the one shown in yellow as it is the one with the shortest delay (158.5 ns) and at the same time strongest power level (-90.1 dBm), as seen in the colour bar. This path, arrived at the antenna with an elevation of 76º and an azimuth of 318º. The reason why the elevation's value is high is because of the height of the antennas, as the receiver antenna is 3m height and the transmitters are 1 m height. The azimuth's value is totally reasonable with the definition of the azimuth's reference, as this UE location is in LOS with the BS and due to that, its value should be between 270º and 360º, and in this case the azimuth is 318º, which satisfies the previous condition.

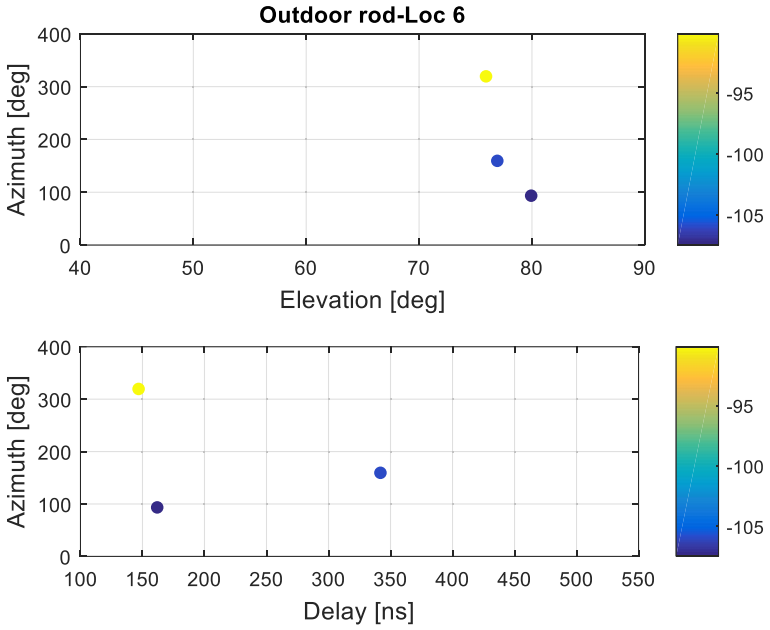

Figure 14. Multipath at the 6th UE location in the 2nd case.

We can also check the effects of the obstacles by taking a look at the next figure. Figure 15 shows the presence of one unique path arriving at the second UE antenna location, which is placed farther than the sixth one. The reason for this is because the emitted signal does not suffer from any significant kind of reflection, or in case it does, its magnitude level is smaller than the power threshold due to the fact that the signal attenuates with the distance as we saw before in Section 2.7. Indeed, this power threshold has been considered in each of the UE locations and it has been defined as 30 dBm down from the highest peak of each UE location.

In other words, we may be receiving more paths but as its power levels are smaller than the threshold limit defined, we don't consider them in the study. In other words, if we compare this result with the previous one, we can notice the multipath effects, as the farther the antenna is, less and weaker paths are received.

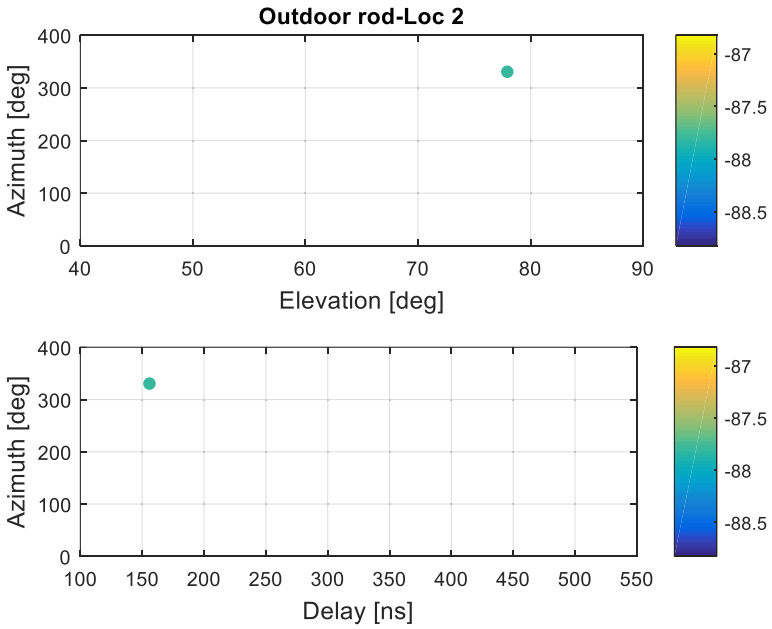

Figure 15. Multipath at the 2nd UE location in the 2nd case.

However, in the next figure, Figure 16, we can see an example of a NLOS UE location, where the ray with the strongest power, -106.5 dBm, (shown in yellow) is not the ray which arrives the first one at the UCA (actually this one has a power of -112.6 dBm). This is due to the multipath effect, in other words, the path with the strongest power level arrived 25 ns later than the first one due to some probable constructive reflections while the path that arrives the earliest has probably been diffracted along its propagation trajectory. Regarding the strongest path, its 90º of elevation and 230º of azimuth at a minimum distance of 66.78 m can be only explained by a reflection of the ray in the walls named 'C' and 'B' (see Figure 3).

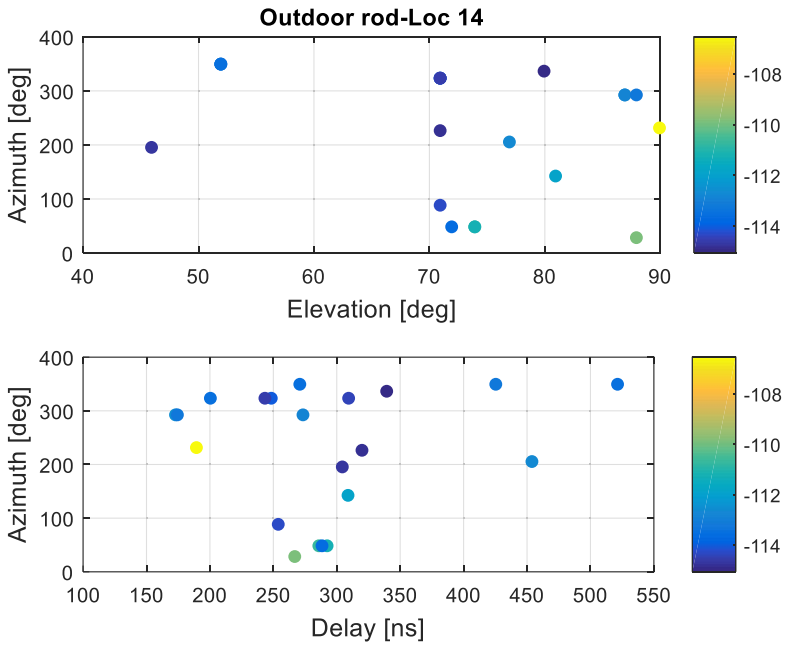

Figure 16. Multipath at the 14th UE location in the 2nd case.

In Appendix 1 and Appendix 2 all the results from all the different antenna locations are represented for the 1st case and for the 2nd case respectively.

In the next figure, Figure 17, we can appreciate the overall number of rays that arrive at each UCA in each scenario and its estimated power delay profiles. On the left of that figure it is shown the 1st case scenario and on the right the 2nd case. From now on, all the results shown and discussed below were all obtained from our own MATLAB code, which, as we have already mentioned, can be found in Appendix 3.

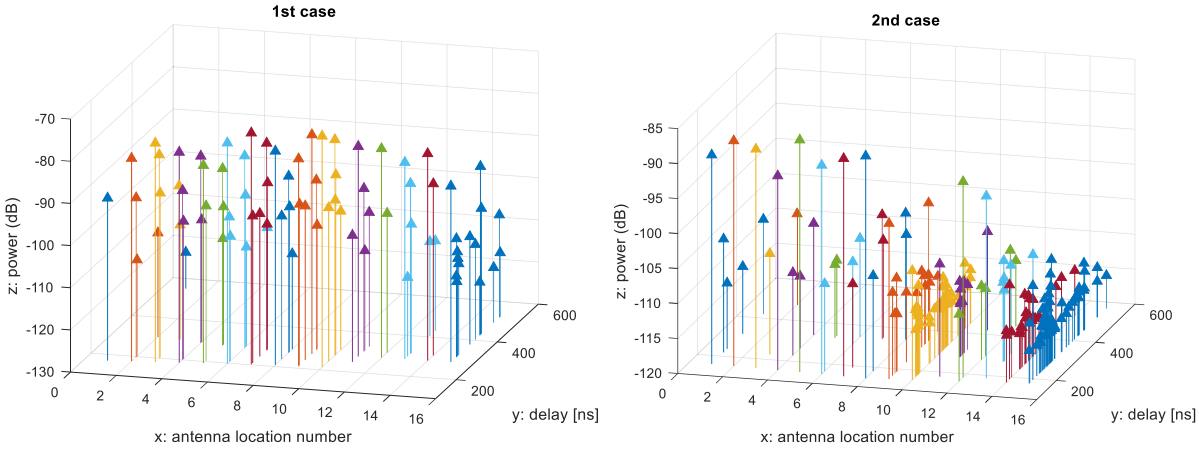

Figure 17. 3D-View of the 1st and 2nd scenarios.

Moving on, in Figure 18 is represented the 1st case scenario, the one where the BS is located on the roof. As we have already mentioned, from this figure we can see that in this 1st case, the farther the UCA is, the more paths are received in each location due to the multipath propagation and the presence of obstacles. The delay and the spread also tend to increase with the locations. Regarding the power across locations, and consequently the path loss values, we can see from Figure 18 that these are not consistent. The view on the right of that figure represents the power from all the paths received for each antenna location. As it can be seen, even though the first antenna location is in LOS and has the shortest delay, it has the weaker power, which is totally unexpected under this situation.

From the view on the left of Figure 18, we can notice the LOS paths, and some possible reflections or double reflections. These reflections or double reflections cause shorter delays from locations 2 to 8 despite the link distance increases, as it can be observed from the LOS path delay. As it can be seen, the locations that are in LOS with the BS are the ones from the first UE location until the tenth one.

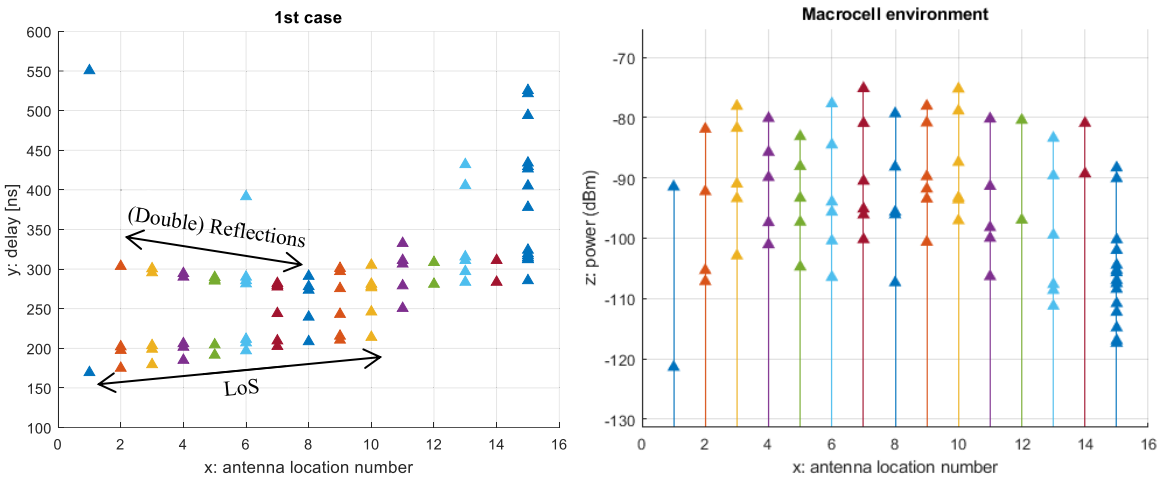

Figure 18. BS on the roof, 1st case.

In Figure 19 it is shown the 2nd scenario, the one where the BS is placed on the rod. As we can see in this case, there are more reflections than in the previous one due to the height of the BS (as it is 17 m lower than in the previous scenario) and the conditions of the medium (we can see from Figure 3 that when the BS is placed on the rod there are more obstacles affecting the propagation channel than when the BS is placed on the roof, and indeed, these obstacles are closer to the UE antennas nearby the BS). These two main considerations affect also to the received power which losses intensity, and if we compare it with the previous scenario, it is

around 10 dB smaller. In this case, we can see that the locations which are in LOS with the BS are the ones between the first UE location until the eight one.

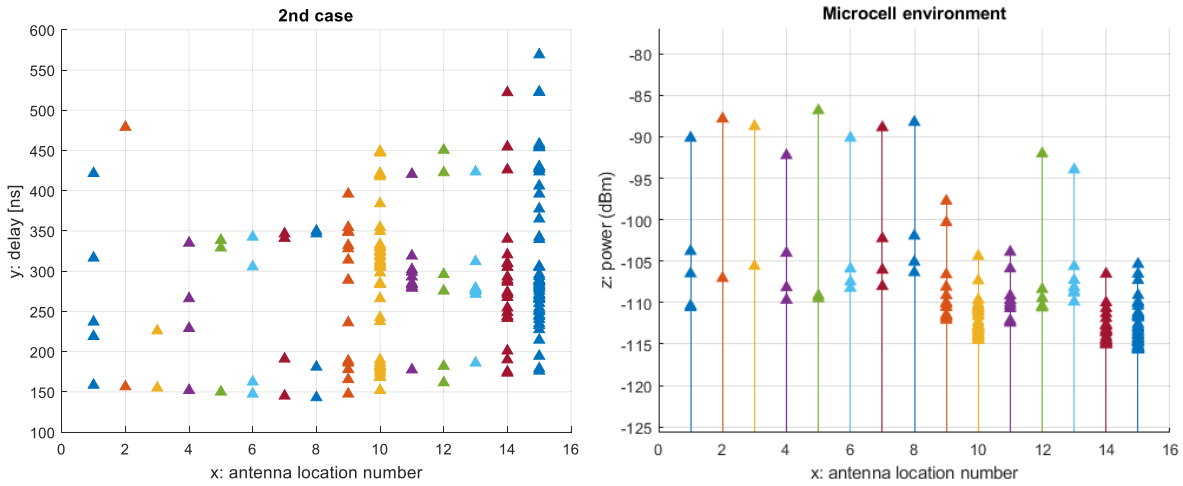

Figure 19. BS on the rod, 2nd case.

4.1.2 Pathway analysis

In order to calculate the origin of the reflections we have mentioned before, we carried out an analytic method in which we have estimated the route of each path by previously knowing its total delay, its azimuth and elevation values, and the real dimension of the scenario (this is explained right after Figure 20). From this analysis, we have calculated the trajectory of the paths and after that we have drawn some of them in Figure 20. Indeed, for the 1st case scenario, we could check that all the UE locations between the first one until the tenth one included, were in LOS, as its first path was a direct path, while the rest of the paths that were received came from previous reflections in different walls or other obstacles. Regarding the 2nd case, the UE locations that received a direct path were the ones between the first one until the eighth UE location, so once again these were the locations that were in LOS with its BS, being the rest of the locations in Non Line-Of-Sight (NLOS) condition.

In Figure 20 we have drawn some of the interaction points the most accurate as possible for both cases under study. We can see some of the different paths through which the signal travels through until it reaches a certain UE location. For example, if we consider the 1st case, we can see that for the 3rd UE location, which is in LOS with its BS, the first path that is received (yellow continuous line), comes directly from the BS while the second path (yellow discontinuous line), comes from a reflection in 'Wall A', just as we introduced before. If we

look again at Figure 20, we can also see for that same 1st case but 8th UE location, that we have the same situation, the first path (blue continuous line) arrives directly at the antenna while the second path (blue discontinuous line) reflects previously in 'Wall B' and then reaches the eighth UE location.

Related to the 2nd case, we would like to analyse for example the 6th and 11th UE locations. As we have already mentioned, the 6th UE location is in LOS condition so it has a direct path arriving to it (green continuous line). However, the 11th UE location does not receive any direct path as it is in NLOS condition. Due to this, the paths that this UE location receives (green discontinuous line), come from previous reflections in 'Wall C' or others.

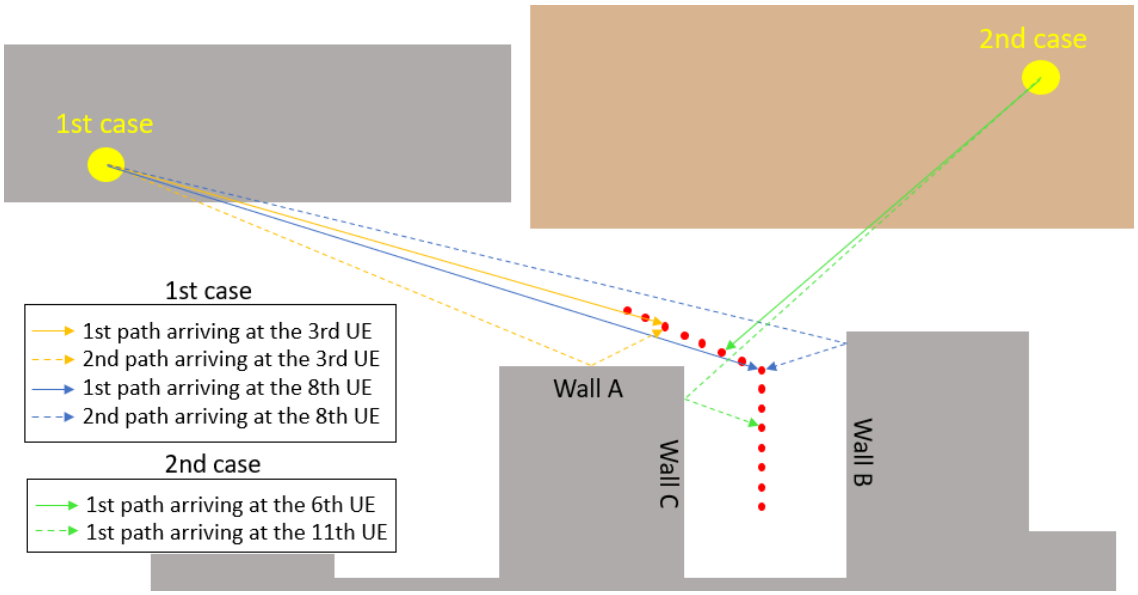

Figure 20. Route of the paths.

As it can be seen from Figure 20, all the reflections follow Snell's law. This principle states that the ratio of the sines of the angles of incidence and refraction remains constant for all incidences in any media for electromagnetic waves [14]:

$$n_1 * sin(\theta_1) = n_2 * sin\,(\theta_2)\,, \tag{13}$$

where n_1 and n_2 are the refraction indices of the two materials and θ_1 and θ_2 are the angles of incidence and refraction respectively [9].

Details of the way these routes were calculated are indicated below:

1. The first step consists of measuring the possible distance between the BS and one of the UE locations number from the map (see Figure 3). Focussing on the first case under study, the 3rd UE location, we can see that the distance from the map in this example is:

$$d_1' = 5.9 \text{ cm} ,$$

In case we have a path coming from a reflection, we have to measure the two (or more) possible distances. For example, for the second path we have discussed before (the yellow discontinuous line), we would have the following distances if we consider that the path reflects in 'Wall A':

$$d_1' = 6 \text{ cm} ,$$
$$d_1'' = 0.9 \text{ cm} .$$

In this step, in order to guess where the path comes from, it is important to focus on the azimuth and elevation values, and see if those results make sense with the path we have probably found. If the azimuth and elevation values are not coherent with the hypothetical route, we should look for a different trajectory.

2. The second step is about converting the d_1' and d_1'' distances into a metre scale distance. This is done by knowing that 19.2 m corresponds to 2.3 cm on the map (see Figure 3 and Figure 5). We also need to consider the height difference between the BS and the UE, *h*, so in order to calculate the real distance between the antennas we need to apply Pythagoras' equation:

$$d_1 = \sqrt{h^2 + \left(\frac{19.2}{2.3} * d_1'\right)^2} \text{ (m)} , \tag{14}$$

Applying this equation to our example we obtain that d_1 is 53.16 m.

In case we have a path coming from one or more reflections, we would apply the following equation, which gives us a distance of 61.45 m for the second path (yellow discontinuous line):

$$d_1 = \sqrt{h^2 + \left(\frac{19.2}{2.3} * d_1'\right)^2} + \left(\frac{19.2}{2.3} * d_1''\right)^2 + \cdots \text{ (m)} . \quad (15)$$

3. The third step consists on calculating the distance by previously knowing its total delay parameter. This is done by multiplying that total delay value, τ, by the speed of light, c:

$$d_2 = \tau * c \text{ (m)} . \quad (16)$$

   Applying this equation to our example, we get that d_2 is 53.81 m for the direct path (which its τ value is 179.5 ns), and 59.66 m for the one coming from a reflection in 'Wall A' (which its τ value is 199 ns).

4. At this point, we just need to compare the distances obtained in the second and the third steps. If these distances are similar, we can completely assure that we have found the real route of the path, but if the distances are not similar, we need to go back to the first step and find a different route on the map.

The excel file with the steps, calculations and results followed in this method for different UE locations can be seen in Appendix 4.

4.1.3 Measures out of the estimation

Once we have analysed the trajectory of each path, we proceed to estimate the delay and azimuth spreads, as defined in Sections 2.3 and 2.6, and the path loss, mentioned in Section 2.7. These results are shown in Table 4, where we can also see, for each scenario, the number of paths arriving at each antenna location and for each of them its path loss value. The mean values of the number of rays, delay and azimuth spreads and path loss can be found at the bottom of the table.

Regarding the path loss, we would like to highlight the way it was calculated. As we have already mentioned, we have summed up, in natural units, all the received powers of each path that satisfied a certain threshold limit (explained in Section 4.1.1) for each UE location, as seen in the equation below:

$$P_{R_{i^{th}UE}} = (A_{1^{st}path})^2 + (A_{2^{nd}path})^2 + \cdots + (A_{k^{th}path})^2 , \quad (17)$$

where $P_{R_{i^{th}UE}}$ is the received power at a certain UE location, i is one of the 15th different UE locations, A represents the amplitude of each path, and k is the last path that meets the threshold's limit.

Once we have the received power, we can then obtain the path loss value, PL, by just applying the following equation:

$$PL_{i^{th}UE} = 10\, log_{10}(P_{R,\, i^{th}UE}) , \quad (18)$$

Table 4. Results

UCA location number	Number of paths		Delay Spread (ns)		Azimuth Spread (º)		Path Loss (dB)	
	1st case	2nd case	1st case	2nd case	1st case	2nd case	1st case	2nd case
1	2	5	12	42	14.3	49.5	91.5	89.8
2	4	2	10	35	28.0	41.6	81.5	87.8
3	5	2	18	10	48.9	41.9	76.3	88.7
4	5	4	42	46	49.0	55.9	78.6	91.8
5	5	3	40	19	38.6	52.5	81.5	86.8
6	7	4	33	36	49.4	48.9	76.7	89.9
7	6	4	32	47	36.0	53.8	74.0	88.6
8	5	4	22	48	33.0	51.6	78.6	87.9
9	6	14	32	93	51.9	52.8	75.8	94.2
10	6	37	30	92	38.6	53.7	73.4	95.9
11	5	10	10	84	49.5	52.6	79.8	98.7
12	2	6	4	48	46.7	52.6	80.3	91.7
13	6	8	15	52	49.3	51.6	82.4	92.9
14	2	22	9	84	46.3	37.7	80.3	99.0
15	15	50	71	94	56.4	22.7	85.6	95.4
Mean	5.4	11.7	25	55	42.4	48.0	79.7	91.9

Once we have the results from Table 4, in the next sections we will proceed to analyse the validity of the delay spread, azimuth spread and path loss results.

4.1.3.1 Delay Spread

To begin with, we first validate the delay spread results by comparing the results we have obtained (see Table 4) with the average values that are mentioned in the reference extracted from the 3GPP specifications [15]. In that reference it is mentioned that for a macrocell outdoor environment, which would represent the 1st case scenario, the rms delay spread, $S_{d\,Uma}$, at 29 GHz for LOS condition should be around 80 ns and 264 ns for NLOS condition. These results have been calculated by applying the equations shown below (19) and (20) at a carrier frequency of 29 GHz [15]:

$$S_{d\,Uma\,LOS}\,(ns) = (10^{-6.955-0.0963\,log_{10}(f_c)}) * 10^9 = \text{ 80 ns}, \tag{19}$$

$$S_{d\,Uma\,NLOS}\,(ns) = (10^{-6.28-0.204\,log_{10}(f_c)}) * 10^9 = 264 \text{ ns}. \tag{20}$$

If we take a look at Figure 21 and focus on the 1st case, we can see that the values achieved in our study are a bit different from the ones obtained through the reference model. We have obtained values of around 27 ns in LOS condition (pink shadow, from the 1st until the 10th location) and around 22 ns and in NLOS condition (blue shadow, from the 11th until the 15th location). This information is collected in Table 5. One of the reasons that may justify this difference is the short distance between the antennas, as we can see from Figure 21 that the delay spread is maximum in the 15th UE as it is the furthest UCA placed and at the same time it is the one that receives more multipath components. We should also consider that we are not working in a typical urban environment with regular streets and building grids, in other words, in our scenario we do not have as many obstacles as a normal urban environment would have (see Figure 3).

This reference [15], also specifies average values for a microcell outdoor area, which would correspond to the 2nd case scenario. In this case, the reference rms delay spread values, $S_{d\,Umi}$, that should be obtained at a carrier frequency of 29 GHz are calculated by applying equations (21) and (22) [15]:

$$S_{d_{Umi\ LOS}}(ns) = (10^{-0.24\,log_{10}(1+f_c)-7.14}) * 10^9 = 32 \text{ ns}, \quad (21)$$

$$S_{d_{Umi\ NLOS}}(ns) = (10^{-0.24\,log_{10}(1+f_c)-6.83}) * 10^9 = 65 \text{ ns}. \quad (22)$$

As we can see from those results, for a LOS condition we should have a rms delay spread value of 32 ns while in a NLOS condition this value should be around 65 ns. If we look at Figure 21 and focus on the 2nd case, the values that we have obtained in this study are approximately about the same level: in LOS condition (pink shadow, from the 1st until the 8th location) we have obtained values of around 35 ns, and in NLOS condition (blue shadow, from the 9th until the 15th location) around 78 ns, so we can assure the validity of our results. This information is collected in Table 5.

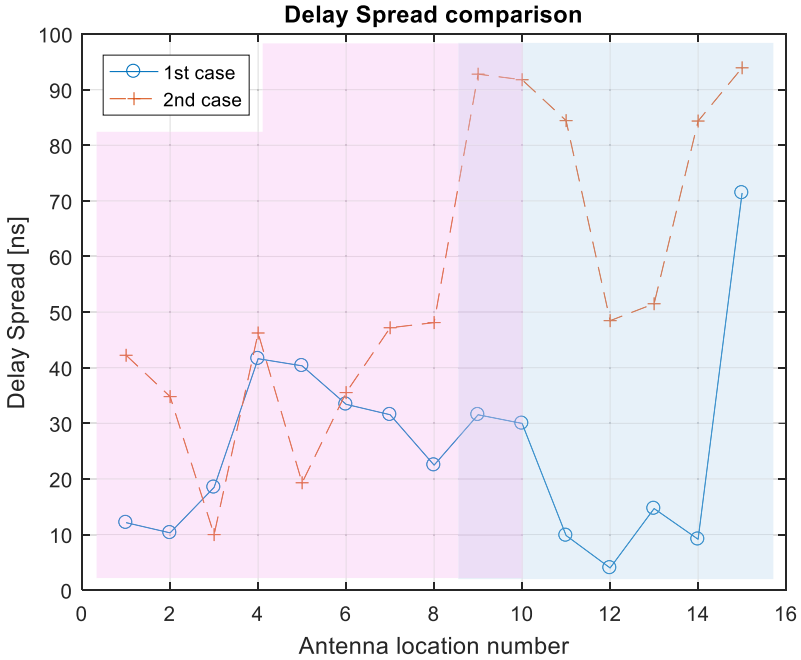

Figure 21. Delay spreads comparison (pink shadow represents LOS for the 1st case and blue shadow represents NLOS for the 2nd case).

Table 5: Delay Spread comparison

Scenario		3GPP results at f_c = 29 GHz (ns)	Mean values obtained from Figure 21 (ns)
1st case	LOS (from the 1st until the 10th location)	80	≈ 27
	NLOS (from the 11th until the 15th location)	264	≈ 22
2nd case	LOS (from the 1st until the 8th location)	32	≈ 35
	NLOS (from the 9th until the 15th location)	65	≈ 78

As we can see from this section, in our study the delay spread obtained from the 1st case resembles more of microcell rather than macrocell environment just as we have already explained.

Once we have analysed these results, the next figures show exactly what we can obtain if we run our MATLAB code. As it can be seen, the program calculates and compares the results with the reference values automatically, just as we have already mentioned in this section. This is done by defining only the central frequency of interest, the amount of receiver antennas, and the distances between the transmitter and the receivers. It is important to mention that the code differentiate between LOS and NLOS distances, so the distances should be specified in that way, and we would also like to mention that our MATLAB code is implemented for just one transmitter. Through our MATLAB code, we can also specify if we are in a macrocell or microcell environment and the power threshold limit used for all the delay and azimuth spread calculations, and also for the path loss calculations, as we described before in Section 4.1.1. Finally, we can also modify the maximum number of paths that arrive at the receiver antennas, indeed, in this study it was set to 50.

As we have just introduced, the next figures show the results obtained from our MATLAB code in our cases under study. On the left of Figure 22 we can see the case of a macrocell environment, which is our 1st case, and on the right of Figure 22, a microcell's environment, which is our 2nd case.

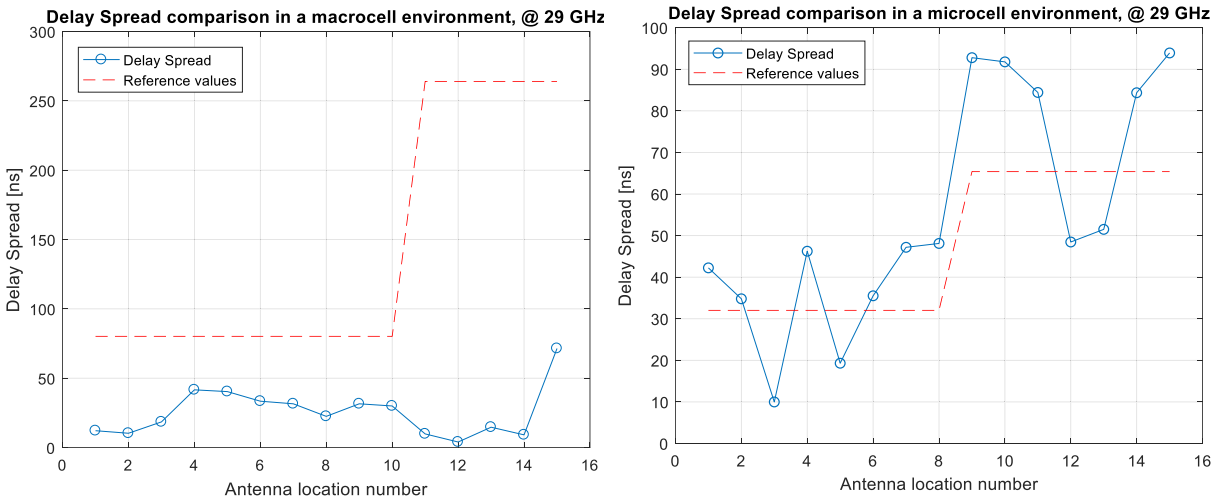

Figure 22. MATLAB's results from the delay spread in a macrocell environment (on the left) and microcell environment (on the right).

4.1.3.2 Azimuth Spread

In relation to the azimuth spreads, we are going to proceed in the same way as we have done with the delay spread in order to see whether the results we have obtained seem reasonable or not. We have also taken into account the 3GPP specification [15] as it provides the correct average values for each scenario.

Starting with the 1st case, the 3GPP reference specifies that the Azimuth Angle of Arrival (AoA) $S_{a_{Uma}}$, for a LOS condition should be 65º, and for a NLOS condition it should be 48º. These results have been calculated by applying the equations shown below (23) and (24) at a carrier frequency of 29 GHz [15]:

$$S_{a_{Uma\ LOS}}(º) = 10^{-1.81} = 65º\,, \tag{23}$$

$$S_{a_{Uma\ NLOS}}(º) = 10^{2.08-0.27\,log_{10}(f_c)} = 48º\,. \tag{24}$$

Analysing these results with the ones obtained in our study (see Figure 23) and focussing on the first case, we proceed to validate our results. In LOS condition (pink shadow, from the 1st until the 10th location) we have obtained a result that differs from its reference value by 26º (the reference value is 65º and the value we have obtained is 39º). The reason for this is that in this particular scenario, in LOS condition and due to the characteristics of the environment, not

many paths are received (the average in LOS is 5 paths received per antenna location), and as a consequence, the angular spread is smaller. However, we can confirm that the values we have obtained are approximately about the same level for the NLOS condition (blue shadow, from the 11th until the 15th location), where there is barely no difference between the reference value (48º) and the one we have obtained (50º). This information is collected in Table 6.

This reference also specifies information for a microcell environment, which corresponds to our 2nd case in the study. In this case, the reference AOA that is obtained at a carrier frequency of 29 GHz have been calculated by applying the equations (25) and (26), for LOS and NLOS conditions respectively [15]:

$$S_{a_{Umi\ LOS}}(º) = 10^{-0.08\,log_{10}(1+f_c)+1.73} = 41º\,, \tag{25}$$

$$S_{a_{Umi\ NLOS}}(º) = 10^{-0.08\,log_{10}(1+f_c)+1.81} = 49º\,. \tag{26}$$

Analysing again our results, we can see from Figure 23 and focussing this time on the 2nd case, we can confirm that the results seem reasonable as they are about the same level. In LOS condition (pink shadow, from the 1st until the 8th location) we have obtained values of around 50º which implies a difference of 9º respect its reference value, and in NLOS condition (blue shadow, from the 9th until the 15th location) around 46º, which is a difference of 3º respect its reference value. In this way, we can also assure the validity of our results. This information is collected in Table 6.

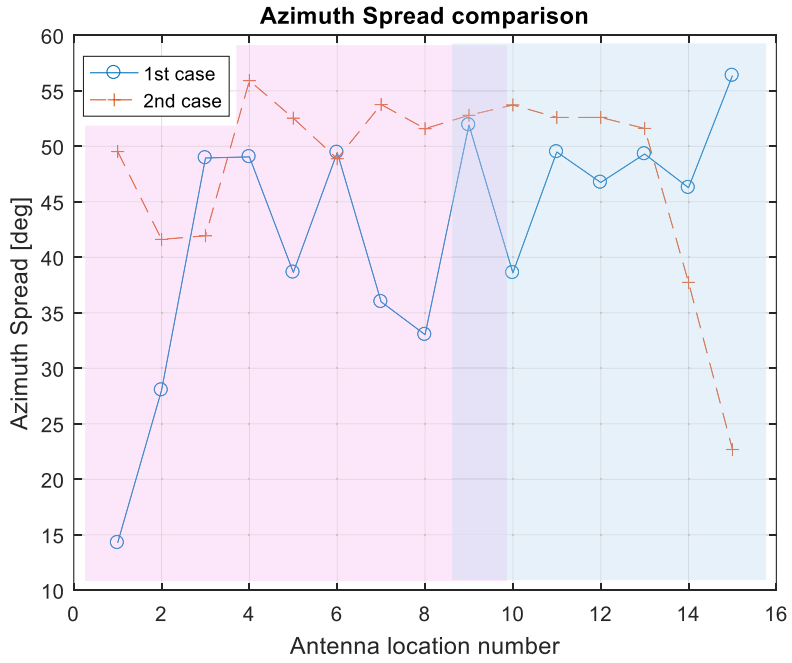

Figure 23. Azimuth spreads comparison (pink shadow represents LOS for the 1st case and blue shadow represents NLOS for the 2nd case).

Table 6: Azimuth spreads comparison

Scenario		3GPP results at f_c = 29 GHz (º)	Mean values obtained from Figure 23 (º)
1st case	LOS (from the 1st until the 10th location)	65	≈ 39
	NLOS (from the 11th until the 15th location)	48	≈ 50
2nd case	LOS (from the 1st until the 8th location)	41	≈ 50
	NLOS (from the 9th until the 15th location)	49	≈ 46

Just as we have done in the previous section, if we run our MATLAB code we can then obtain the results shown in Figure 24, which shows a comparison between our results and the reference values, for the 1st case, on the left, and the 2nd case, on the right, under study, just as we have mentioned in this section.

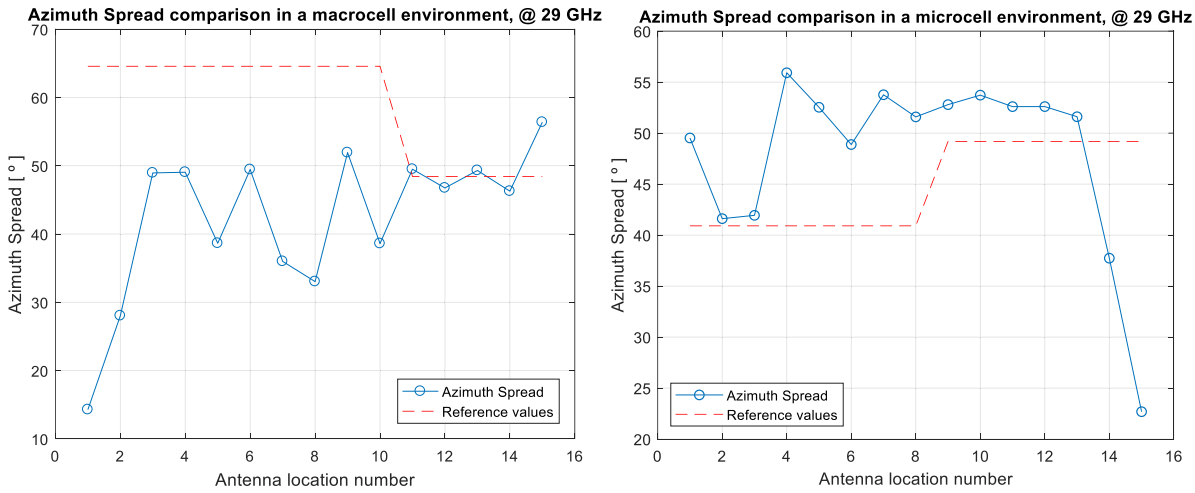

Figure 24. MATLAB results, azimuth spread in a macrocell environment (on the left) and microcell environment (on the right).

4.1.3.3 Path Loss

In this subsection, we are now going to analyse the validity of our path loss values. In LOS condition, this is done by calculating the free space loss for both cases, and then comparing it with our results. This is done by applying the equation (27). As it can be seen below, this equation depends only on the carrier frequency, f_c, (in GHz) and on the distance, d, (in km) between the transmitter and receiver [7]:

$$L_{bf} = 92.44 + 20\,log(d) + 20log\,(f_c)\,. \tag{27}$$

By doing this for both cases, we have obtained the values shown in Table 7 (for the 1st case) and Table 8 (for the 2nd case). In those tables we can see, for each UE location that is in LOS condition, the distance covered by the LOS path, its path loss values (which are the same ones as the ones calculated in Table 4), the reference values obtained from the free space loss model (equation (27)), and the difference between our values and the reference ones.

By taking a look at Table 7, we can see that for the first case under study, the difference between the reference values (free space loss) and our values, is around 18 dB for all the locations. This deviation is too high to be only explained by the environment, so measured path loss values are evidently inconsistent. Indeed, and as we have already discussed in Section 4.1.1, the fact that the first antenna, which is in LOS and has the shortest delay, receives the weakest power level

is incongruous. With all of this we can conclude that there has been an unknow effect in the measurement or calibration that makes path loss non-comparable.

Table 7: Path loss results, LOS condition for the 1st case

LOS	UE locations	Distance d_2 (m)	Path Loss values (dB)	Free space loss (dB)	Difference (dB)
1st case	1	50.81	91.5	95.8	4.3
	2	52.46	81.5	96.1	14.6
	3	53.81	76.3	96.3	20.0
	4	55.46	78.6	96.6	18.0
	5	57.41	81.5	96.9	15.4
	6	59.06	76.7	97.1	20.4
	7	60.71	74.0	97.4	23.4
	8	62.51	78.6	97.6	19.0
	9	63.11	75.8	97.7	21.9
	10	64.16	73.4	97.8	24.4
	Mean				18.1

These results are plotted in the next figure, Figure 25, where we can see the path loss results obtained from running our MATLAB code. This figure also has information related to the results obtained from the NLOS condition (equation (28)), which will be analysed during this section. As it can be seen, the results from our study are shown in a blue continues line, while the results from the reference models (which are obtained from equation (27) for LOS condition, and equation (28) for NLOS condition) are shown in a red dashed line.

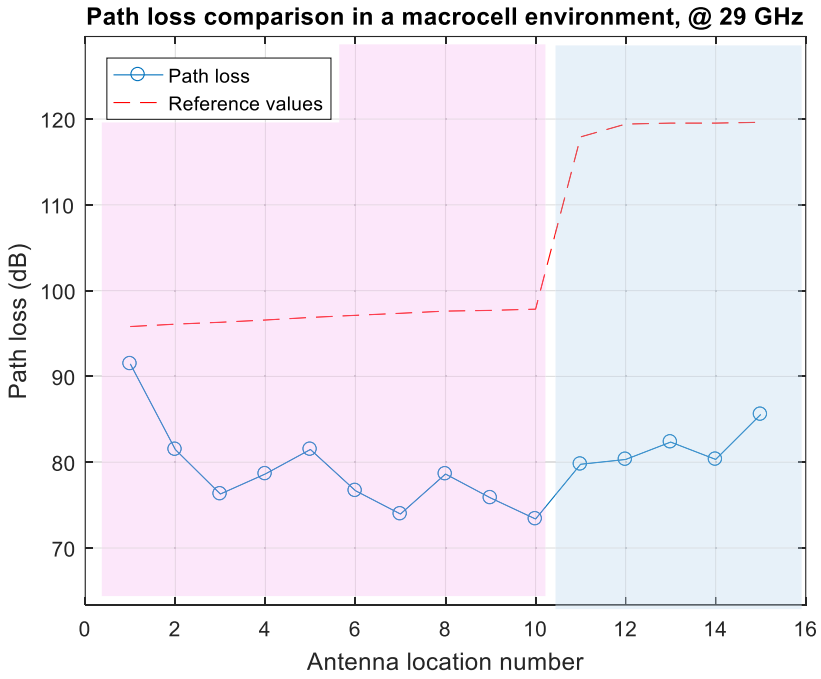

Figure 25. Path loss comparison 1st case (pink shadow represents LOS and blue NLOS).

However, if we analyse now the LOS condition for the second case, we can notice that the deviation between the free space loss and our values is of around 6 dB, as it can be seen from Table 8. This result is 12 dB smaller than the one obtained in the 1st case (where we had a difference of 18 dB) so we can validate our results. Despite we can do so, we should remark that this difference is also justified by the characteristics of our environment, as we do not really have as many buildings or obstacles obstructing the propagation path as a normal urban environment would have.

Table 8: Path loss results, LOS condition for the 2nd case

LOS	UE locations	Distance d_2 (m)	Path Loss values (dB)	Free space loss (dB)	Difference (dB)
2nd case	1	47.52	89.8	95.2	5.4
	2	46.92	87.8	95.1	7.3
	3	46.47	88.7	95.0	6.3
	4	45.57	91.8	94.9	3.1
	5	44.97	86.8	94.8	8.0
	6	44.22	89.9	94.6	4.7
	7	43.47	88.6	94.5	5.9
	8	42.87	87.9	94.3	6.4
	Mean				5.9

These results are also plotted in the next figure, Figure 26, where we can see the path loss results obtained from running our MATLAB code. Just as we mentioned in the previous case, this figure also has information related to the results obtained from the NLOS condition (equation (29)), which will be analysed during this section. As it can be seen, the results from our study are shown in a blue continues line, while the results from the reference models (which are obtained from equation (27) for LOS condition, and equation (29) for NLOS condition) are shown in a red dashed line.

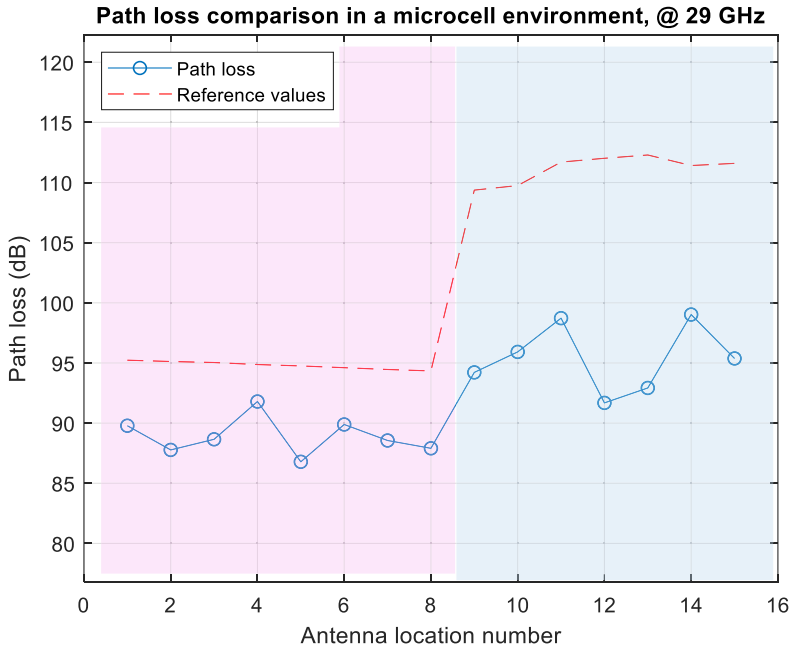

Figure 26. Path loss comparison 2nd case (pink shadow represents LOS and blue NLOS).

Once we have analysed the LOS condition, we proceed to study the NLOS situation for both cases. Just as we have done with the LOS condition, we are going to compare our values with some reference results. In this case, we cannot compare our results with the ones from the free space loss (equation (27)), as this is only feasible for LOS condition. Thereby, the reference values could be obtained either by calculating the Close-In (CI) Free Space Reference Distance Model or by applying the Alpha-Beta-Gamma (ABG) Model. Despite both models describe large scale propagation path loss at any frequency and in any scenario, [16], we are going to use the first one as it provides good estimation and provides more stable behaviour across frequencies and distances, [17].

In [18] we can find the equations needed for calculating the path loss reference values in dB. These equations can be seen below, where (28) applies to a macrocell environment (1st case) and (29) to a microcell environment (2nd case). Regarding the microcell environment, we would like to mention that we have chosen the open street model, OS, rather than the street canyon model, SC, due to our environment characteristics because, as we have already mention, we do not have as many buildings and obstacles as a normal urban area would have:

$$PL_{CI\,Uma} = 32.4 + 30\,log_{10}(d) + 20\,log_{10}(f_c), \qquad \sigma = 6.8 \text{ dB}, \tag{28}$$

$$PL_{CI\,Umi\,OS} = 32.4 + 29\,log_{10}(d) + 20\,log_{10}(f_c), \quad \sigma = 7.1 \text{ dB}, \tag{29}$$

where the distance d is in metres, the carrier frequency, f_c, in GHz, and σ is the standard deviation.

In the next table, Table 9, we can see, for each UE location that is in NLOS condition, the real distance between the antennas, its path loss values (which are the same as the ones we obtained in Table 4), the reference values obtained from the CI model (equations (28) and (29)), and the difference between our values and the reference ones for the first case under study. In this way, we can see that the difference between the reference values and our values is around 35 dB. Once again, this deviation is way too high and the only reason we have found out when we analysed the LOS condition, is that there has been an unknow effect in the measurement or calibration that makes path loss non-comparable.

Table 9: Path loss results, NLOS condition, 1st case.

NLOS	UE locations	Distance between antennas (m)	Path Loss values (dB)	Path Loss, CI model (dB)	Difference (dB)
1st case	11	65.83	79.8	117.2	37.4
	12	67.03	80.3	116.4	36.1
	13	67.43	82.4	116.5	34.1
	14	68.63	80.3	116.7	36.4
	15	69.43	85.6	116.9	31.3
	Mean				35.1

As we have already mentioned, these results are plotted in Figure 25, where we can see the path loss results obtained from running our MATLAB code.

Moving on to the study of the NLOS condition from the second case, we can see from the following table, Table 10, that the deviation between the Close-In reference values and ours, is of around 15 dB for all the UE positions. However, we cannot truly validate the measured path loss results since they are inconsistent.

Table 10: Path loss results, NLOS condition, 2nd case

NLOS	UE locations	Distance between antennas (m)	Path loss values (dB)	Path loss, CI model (dB)	Difference (dB)
2nd case	9	42.62	94.2	108.9	14.7
	10	44.29	95.9	109.4	13.5
	11	45.54	98.7	109.7	11.0
	12	46.79	91.7	110.1	18.4
	13	48.46	92.9	110.5	17.6
	14	49.71	99.0	110.9	11.9
	15	50.96	95.4	111.2	15.8
	Mean				14.7

As we have already mentioned, the results from the LOS and NLOS paths are plotted in Figure 26, where we can see the path loss results obtained from running our MATLAB code.

Finally, as we have discussed, it seems that the calibration of this measurement system does not support the absolute path loss evaluation.

4.1.3.4 Elevation

In order to have a better understanding of the problem, we have estimated and then compared the elevation values from our data, and we have found out that there is some kind of error in the measure of the elevation. For the first case, we can see from
Table 11 the results we have obtained from this calculation, which it was done by using geometry as we knew the antenna's height and the adjacent distances between the BS and each UE location. From this analysis we have found out that for some particular UE locations (specially for the 2nd, the 3rd, the 6th and the 10th UE locations) there is a difference of around 11º between the original data and the estimated values. However, if we look at Table 7, we can see that these locations are not necessarily the ones with the largest path loss deviation, so there must be another reason that justifies the path loss inconsistency.

Table 11: Analysis of the elevation, 1st case.

UE location	Elevation angle estimated from the data (º)	Estimated elevation angle derived from the geometry (º)	Difference (º)
1	71	68	3
2	83	69	14
3	81	69	12
4	72	70	2
5	75	71	4
6	82	71	11
7	75	72	3
8	77	72	5
9	74	73	1
10	82	73	9
Mean			6.4

We would like to calculate as well the elevation's measure precision for the 2nd case. In this way, as we also knew the antenna's height and so the adjacent distances between the BS and each UE location, we could estimate again the elevation's angle. As it can be seen from Table 12, on one hand it is true that the estimation is better than in the previous case but on the other hand, this estimation is still not perfect, as for some UE locations, like the 2nd or 6th ones, the difference is too high, 10º and 11º respectively. Looking at the previous results from Table 8, we can see that these locations are, just as in the previous case, not necessarily the ones with the largest path loss deviation, so once again, so there must be another reason that justifies the path loss inconsistency.

Table 12: Analysis of the elevation, 2nd case.

UE location	Elevation angle estimated from the data (º)	Estimated elevation angle derived from the geometry (º)	Difference (º)
1	85	88	3
2	78	88	10
3	84	88	4
4	84	87	3
5	80	87	7
6	76	87	11
7	87	87	0
8	89	87	2
Mean			5

Nevertheless, the next figure represents the simulated normalized elevation plane radiation pattern from the horn antenna at 30 GHz [19]. As it can be seen, a barely 15º difference can easily reduce the elevation plane radiation in 5 dB. This means that an accurate elevation measured is important in order that we can achieve good measurement results. Just as we have already mentioned, we can find the photos from the horn antennas used for the 1st and for the 2nd case in Figure 10 and Figure 11 respectively, where indeed some pointing information is shown.

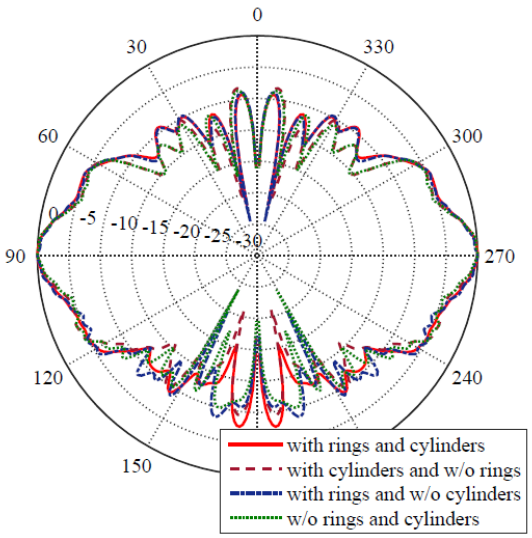

Figure 27. Simulated normalized elevation plane radiation pattern from the horn antenna at 30 GHz [19].

5 VERIFICATION THROUGH KEYSIGHT GCM TOOL

Once we have analysed all the results obtained from MATLAB, the next step in our project is to perform that same investigation but by implementing it through Keysight Geometric Channel Modeling (GCM) Tool.

The aim of this part of the work is to be able to assure the accuracy of the estimations from our analysis, and to reconstruct the channel impulse response through a different tool, that in our case is, as we have already mentioned, Keysight GCM Tool.

5.1 Definition of the scenarios

At this point, the steps followed is to define the two measurement scenarios. For this we will have to define the transmitter and receiver locations, the type of antennas needed, and the estimated propagation parameters. The explanations needed for going through the next subsections can be found in [20].

5.1.1 Locations

The first thing that we have to do is to define our scenarios. In this way we created two different scenarios, one for our first case and the other one for the second case. We would like to highlight that this step was really time-consuming as first, we had to set the antennas in the exact coordinates, which were calculated from the map by following a similar method as the one explained at the end of the Section 4.1.1. Then, we realised that despite the accuracy achieved from the map was really good, those locations were still not the right ones as we were not obtaining the exact same values for our estimated parameters (delay, azimuth and elevation values). We became aware about this as when we defined the locations from the UEs, or MSs, which were in LOS condition, its estimated parameters were automatically calculated and, as a consequence, those values could not be modified. This meant that, the only way we had to change those parameters so they could represent our scenarios was by modifying the MSs' positions until we finally found the right ones from which the LOS parameters made sense with our cases under study. Due to this issue, we had to do some small changes in the MS's positions until we finally found the correct places from which we could obtain the estimated values from our data. In other words, in this measurement report the locations for each MS (where each MS represents one of the UE location positions as we have already mentioned) are not exactly where

they should be based on the reference we had from the measurement data. In that reference we could see, for example from Figure 3 or Figure 4, that those locations were lined up, but nevertheless, the locations that we have chosen for each MS despite they are not aligned, they match with our estimated parameters as we will see in the next figures.

Previously, as we have already discussed, we would also like to mention that the BS's position from the 2nd case was not exactly at the place where the measurement documentation mentioned, so we had to use again our estimated parameters in order to approximate it to its correct coordinates.

Finally, as it can be seen from the figures below, the first figure, Figure 28, shows the scenario for our first case (where the BS is placed on the roof) and Figure 29 shows the scenario for our second case (where the BS is placed on the rod). As it can be seen from those figures, we would also like to mention that through this software we have not specified any blockers' position, which would represent the buildings that we have in our scenarios (see Figure 8 and Figure 9). The reason for this is because this GCM Tool has the 3GPP 38.901 Blockage model A implemented, which means that blockers are random, so we can specify the number and the speed of the blockers but we cannot specify their locations.

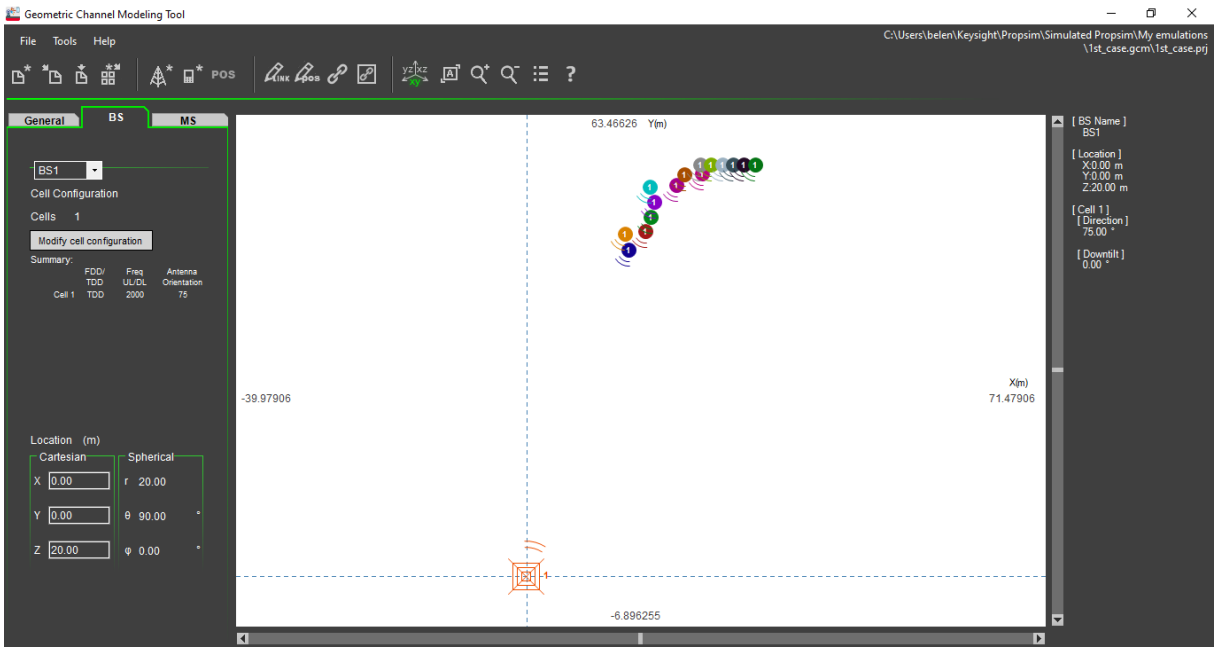

Figure 28. First case scenario.

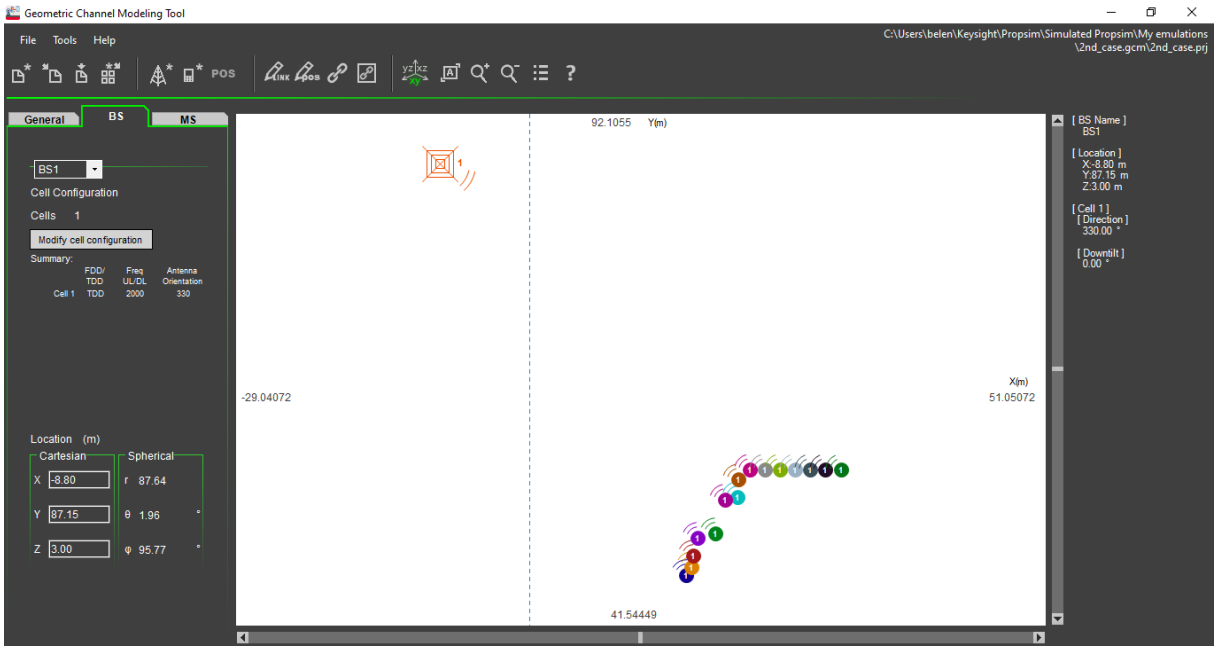

Figure 29. Second case scenario.

5.1.2 Definition of the antennas

Once we have all the BS's and MS's positions well defined, we now need to specify what type of antennas are used for each of them.

Starting with the BS, as we mentioned in Table 3, the type of antenna that was used in our study was a horn antenna. However, as we could not remove the effects that it had in our estimated parameters, if we defined again this BS's antenna as a horn type, we would be introducing twice these horn antenna effects, so this is the reason why we decided to use an isotropic vertical polarized antenna. Finally, we would like to mention that due to this isotropic antenna, it is irrelevant for us to specify the antenna's orientation.

Regarding the MS's antennas, we decided to use vertical polarized dipoles firstly, because they have similar omni-directional radiation patterns as the biconical antennas that we actually used in the study (see Table 3). Secondly, because this antenna type is already defined in GCM Tool while the biconical is not included in the default antenna library. Due to the omni-directional property, it was not important again to define their orientation so we just pointed them to the BS.

After all of this, we would like to highlight that for the MS's antennas, we also needed to characterise our UCAs antennas, which are used in every MS. This was done through the Antenna Array Tool interface. As it can been seen below from Figure 30, for this step we had to select the central frequency (29 GHz), the number of elements (360) and the number of ports (360, one for each element). For each element we also had to specify its x, y and z positions (which were obtained from the code developed for plotting Figure 12), and its x, y and z rotation angles (which were set to 0º for all the elements in order to have a vertical polarized antenna). However, due to the limitation of this interface, we had to cut the UCA into 24 parts, so we could have 15 elements and 15 ports at each part of it. As a consequence, we will see that we had to simulate 24 times each scenario, one time for each UCA's part, and then combine the 24 results together in a way that we get the complete result for the 360 elements of the UCA. In Figure 30 we can see how the top fifteenth elements implemented from the UCA array antenna are defined.

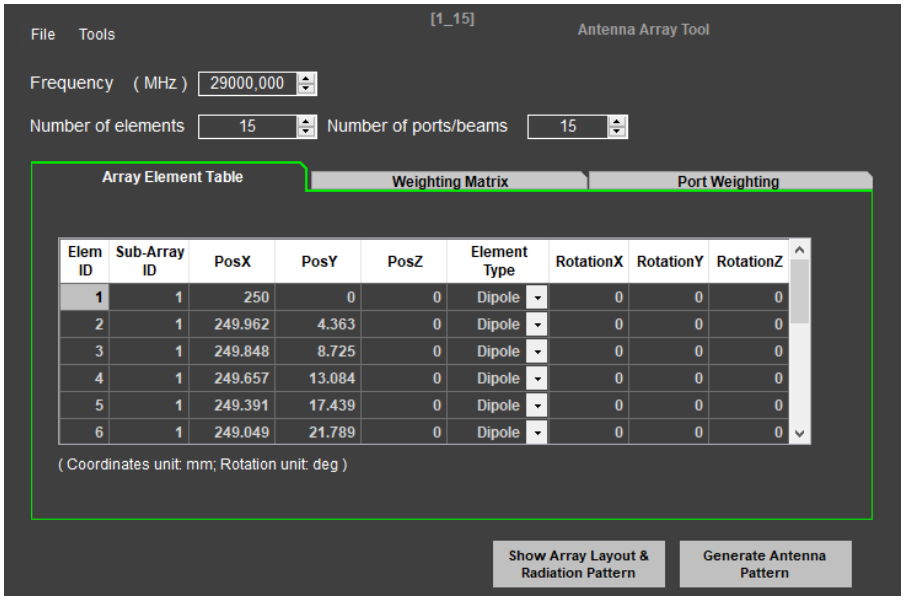

Figure 30. Definition of the top fifteenth UCA's elements.

We would also like to highlight that this part of the work was quite elaborate as through this work we found a bug in Keysight's software and assisted SW development, as the channel matrix export was not working properly when there were fifteenth links in the scenario.

5.1.3 Propagation parameters

Right away we have all the MS and BS positions and antennas well defined, we now proceed to define the remaining propagation parameters so we can create, and afterwards analyse, the scenarios used in the measurement data.

Firstly, we would like to mention that due to the fact that we are only analysing the DL (downlink) transmission, it does not matter whether we use Time Division Duplex (TDD) or Frequency Division Duplex (FDD) but as we had to choose one, we chose TDD.

Secondly, as it can be seen from Figure 32, for each MS, we also need to define the number of clusters that each MS location has. These clusters represent the number of paths arriving at each antenna, and this definition was needed because, as we have already mentioned, we could not define any specific blocker position. This was done by firstly selecting '*User_defined*' as Channel Model and then specifying the number of paths. Through this step we found out that we had a problem as the program only accepted a maximum of 24 clusters. As it can be seen from Table 4, the column named 'Number of paths', there are two occasions in which the number of paths received at a specific MS are higher than 24 (indeed this happens for the MS locations 10^{th} and 15^{th} for the second case). However, despite we thought that by using ray-tracing import we could maybe solve this problem, we found out that we could not. The reason for this is that there were two important requirements that were needed to fulfil when using ray-tracing import. The first one was that it was needed a minimum of 10 multipath components per MS, and the second one was that the maximum number of clusters per MS was still 24. Due to these two conditions, we decided to take the 24^{th} strongest paths and ignore the remaining weaker paths for the two previous MS locations affected by this issue. Indeed, the paths that had to be ignored for these two MS locations were around 10 dB below the strongest path, as it can be seen in Figure 19.

Thirdly, related to the Path loss mode, we had to select '*None'* mode as we did not get a reliable path loss estimation from the measurement. In this way, we have only focussed on relative path's powers within each location, as we will see in the next paragraph.

Fourthly, we had to complete all the parameters shown in Figure 32, in other words, we had to specify the Power, the Excess Delay, the AoA, the Cluster-wise RMS Azimuth Spread of Arrival (ASA), the Azimuth Angle of Departure (AoD), the Cluster-wise RMS Azimuth Spread of Departure (ASD), the Elevation Angle of Arrival (EoA), the Elevation Angle of Departure (EoD), the Cluster-wise RMS Elevation Spread of Arrival (EsA) and the Cluster-wise RMS Elevation Spread of Departure (EsD). Going through these parameters one by one, we would like to highlight regarding the power, and as we have already introduced in the previous paragraph, this parameter is normalized in a way that in LOS condition, the reference used for normalizing the rest of the power's values from the different paths that arrive at a certain MS location, is the power from that same LOS path. The reason for this is because the LOS path is the one with the strongest power value as this path does not suffer from any kind of reflection or diffraction. However, in NLOS condition, due to all the possible reflections and/or diffractions that the paths may suffered from, we cannot assure that the strongest path is the one with the shortest delay. In this way, we decided to use the path with the shortest delay as the referenced one, and normalize the rest of the values respect to that one. This is because in NLOS, the reflected paths have higher gains while the diffracted ones feel shortest path lengths. Indeed, and regarding the LOS condition, there is one occasion in which the LOS path is not the one with the highest energy, so when the rest of the paths are normalized, some of them may result to have a value higher than 0 dB. As this GCM Tool does not support any positive values for the clusters' power parameter, we decided to set those values with 0 dB as well. This incident can be seen in light orange in Appendix 5 for the 1st case and Appendix 6 for the 2nd case, where for example for the first one, we can see that for the 9th MS location, which is in LOS condition, the strongest path is the one that arrives thirdly at the antenna.

Concerning the parameter named 'Excess Delay', we would like to mention that it represents the LOS path delay. In case we are in a NLOS condition, it represents the delay with regard to the path according to the criterion explained before.

Regarding the AoA and EoA, these parameters contain the azimuth and elevation values respectively seen from the MS (the values from our study) while AoD and EoD contain the azimuth and elevation values seen from the BS. Due to the fact that we have not analysed the uplink (UL) propagation path, these values are set to 0º. For AoA and EoA, we would like to mention that as the program used a different reference as the one that the measurement used, we had to convert our original data so that they were at the same reference measurement used in GCM Tool. This can be better seen in the next image, Figure 31, where we can see the

azimuth's and elevation's references used in our original data (which is the one explained in Section 3.2.1) and the reference used in GCM Tool.

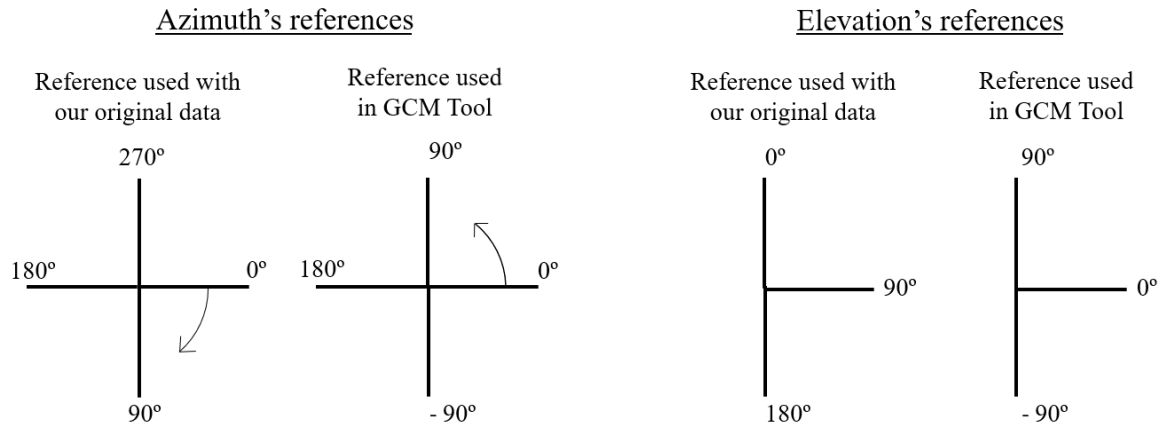

Figure 31. References used.

We would also like to mention again that it is expected some inaccuracy in the EoA's estimations. As we have already discussed, in Section 4.1.3.4 (Table 11 and Table 12) we found out that there was some kind of inconsistency between our elevation's processed data and our elevation's estimations done through geometry. However, as we have just mentioned in Section 5.1.1, for this analysis we had to modify all the MS's positions, which means that all the adjacent distances changed as well, so the previous elevation's estimation accuracy could have changed. To know if these new locations were better than the ones obtained from the map, we have estimated again the accuracy of the elevation's measurement but by considering these new adjacent distances instead of the previous ones. In this way, as it can be seen from Table 13 and Table 14, despite the distances have changed, we still have considerable differences between the given elevation's parameter from our original data and the one from our estimation. However, we have to say that this difference is smaller than before, especially for the 1st case of our study, but as UCAs are not very accurate in the elevation's estimation, we can finally accept these differences. As we have already mentioned, this process, and as a consequence, the results obtained from it which are shown in the tables below, were achieved through geometric rules.

Table 13: Analysis of the LOS elevation from GCM Tool, 1st case

UE location	Elevation angle estimated from the data but in GCM Tool coordinate system, Figure 31 (º)	Estimated elevation angle derived from the geometry of GCM Tool (º)	Difference (º)
1	19	21	2
2	7	20	13
3	9	20	11
4	18	19	1
5	15	18	3
6	8	18	10
7	15	17	2
8	13	17	4
9	16	17	1
10	8	16	8
Mean			5.5
Previous mean			6.4

Table 14: Analysis of the LOS elevation from GCM Tool, 2nd case

UE location	Elevation angle estimated from the data but in GCM Tool coordinate system, Figure 31 (º)	Estimated elevation angle derived from the geometry of GCM Tool (º)	Difference (º)
1	5	2	3
2	12	2	10
3	6	2	4
4	6	3	3
5	10	3	7
6	14	3	11
7	3	3	0
8	1	3	2
Mean			5
Previous mean			5

We would like to remark that despite it has been proved that for these distances we can achieve better EoA's approximations by applying geometric rules, we still have to use the values obtained from our original data. The reason for this is because the aim of our work is to compare the results obtained from our own algorithm when we have the specific input data from University of Aalborg, with the results obtained when we use that same specific input data in this GCM Tool.

Finally, the rest of the parameters (ASA, ASD, ESA, and ESD) are set to 1º as these parameters represent how much spread in angle we have, and in our study, as we have only analysed individual paths, we have not estimated those values.

In the next figures we can see how the interface looks like when we are characterising a MS in LOS condition (Figure 32) and in NLOS condition (Figure 33).

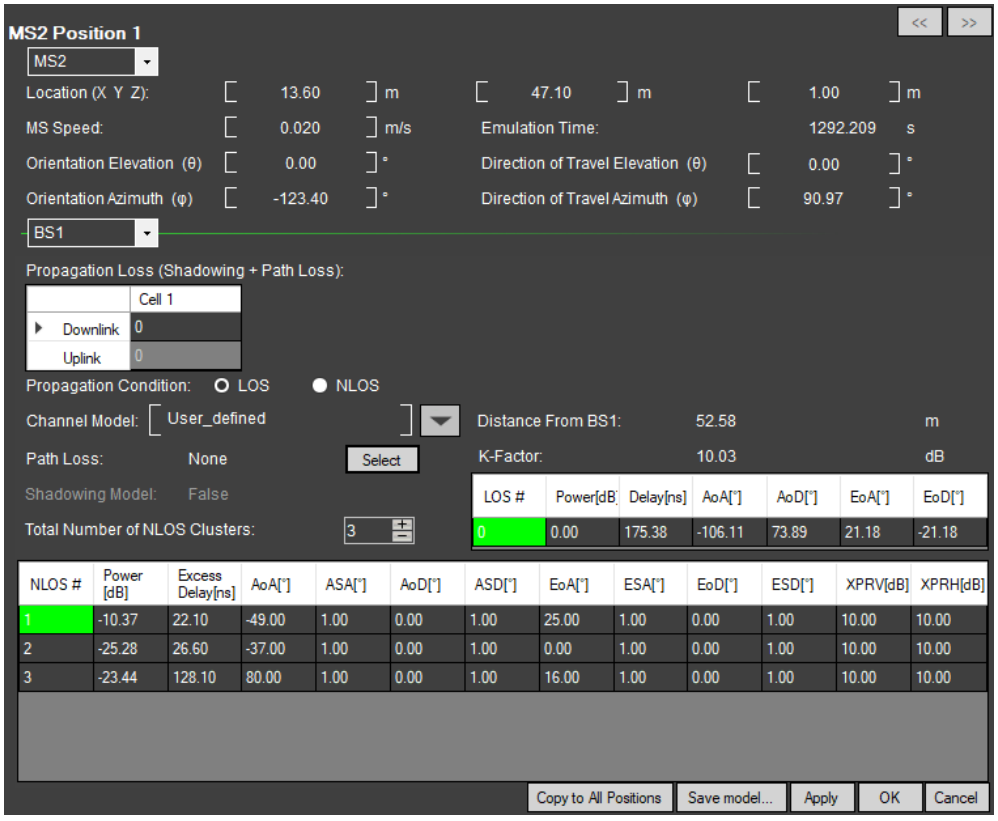

Figure 32. Propagation parameters for the 2nd MS position in LOS condition.

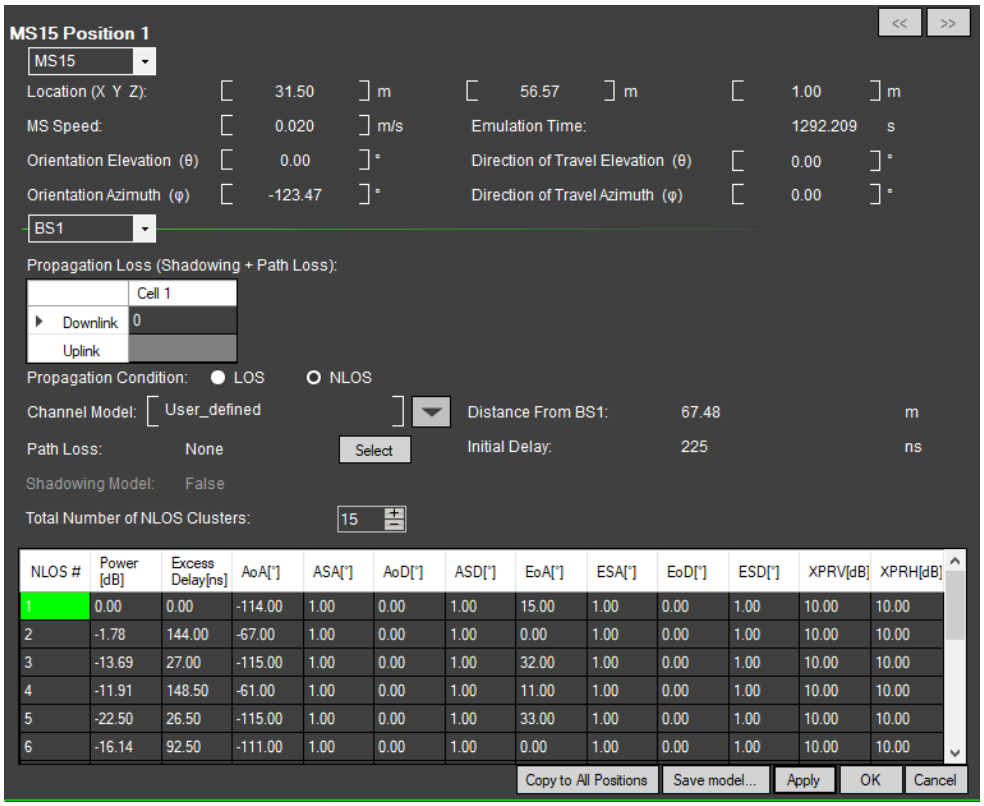

Figure 33. Propagation parameters for the 15th MS position in NLOS condition.

All the values for all the parameters used for the first case can be found in Appendix 5 while the results for all the parameters used for the second case can be found in Appendix 6.

5.2 Performance of the estimation and analysis procedure

Once we have performed the previous section, the second step in this validation process was about generating the channel coefficients and doing the same estimation and analysis procedure for the measurement data just as we did with MATLAB. The aim of this part of the work was then to compare the estimated results obtained from MATLAB with the estimated results obtained from GCM Tool and analyse if those results were reasonable or not, so we could validate the GCM Tool, our estimation model, and the accuracy of our analysis. However, we have not been able to complete this part of the work as during this process we have faced some problems that did not allow us to proceed with our purpose on time. The reason for this is that as we had to adapt channel estimation algorithm MATLAB code for this new purpose, we realised that by adapting it to our new input parameters, we could not read properly neither the azimuth nor the elevation parameters, even though we had the Channel Impulse Response

matrix from each antenna location. The solution of this issue would lead us beyond the timescale of this project.

5.2.1 Analysis of the results

As we have already mentioned, despite we have not been able to estimate the propagation parameters, we do have been able to reconstruct the scenarios with GCM Tool. In this way, once we have carried out the complete 24 simulations for each scenario, we have created the final channel matrix by joining all the results together. Once we have done this, we have been able to analyse the Channel Impulse Response results for each scenario.

Thereby, we are now going to analyse this parameter for the antenna locations closer to the BSs and in LOS with them, as in this way we can get information from both types of propagations paths (LOS and NLOS). Starting with the first case, we are going to analyse the Channel Impulse Response for the 2nd UE antenna location, as this one should have more information than the 1st UE antenna location due to the number of paths that should be received. As we have already seen in Table 4, when we first analysed the propagation path through MATLAB, we realised that the number of paths that were received at this antenna location were four. As we can see from Figure 34, when we plot the Channel Impulse Response obtained from GCM for each delay sample, we can distinguish four different peaks on it. This assures that the channel is being estimated properly as these peaks correspond with the four paths that we had from our previous study (the first peak is at 175.5 ns, the second one is at 197.5 ns, the third one is at 202 ns, and the last one is at 303.5 ns). We would like to emphasize that the power is normalized respect to the LOS path which, as it can be seen below, is the first peak. The fact that the results are normalized with regard to the LOS path is totally reasonable as in order to define the scenario in GCM, we had to normalize the power respect the LOS path.

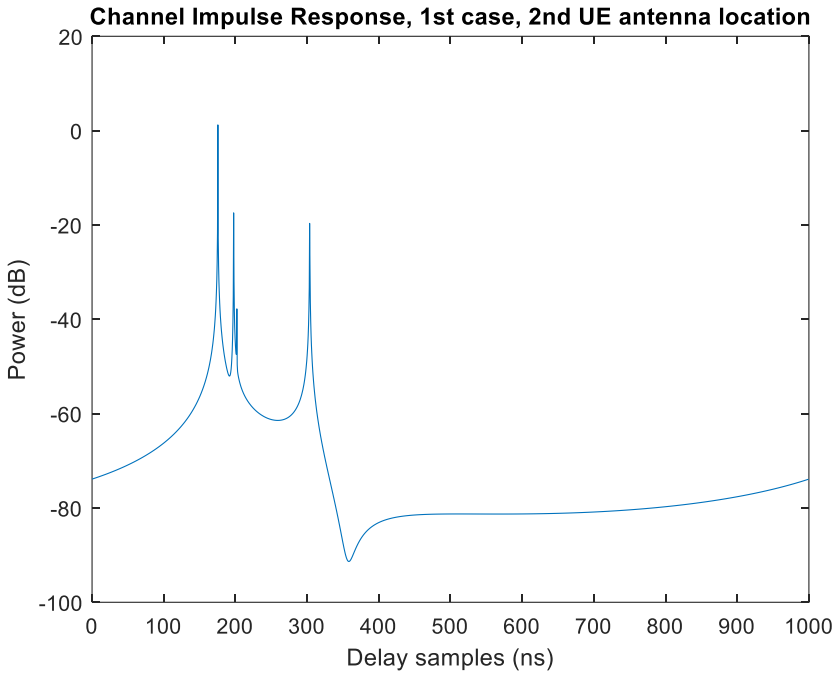

Figure 34. Channel Impulse Response, 1st case, 2nd UE antenna location.

Regarding that same UE antenna location, it is also interesting to analyse how does the phase change among each virtual antenna element from the UCA. Firstly, we would like to emphasize that when the signal arrives at the antenna, due to the distance between the transmitter and the receiver, it comes as a plane wave. By this, when the signal arrives from the horizon, the maximum phase difference between adjacent UCA elements has to be greater or equal than 0º and smaller or equal than 180º. However, if the signal does not come from the horizon, which means that its arrival angle is elevated, this phase difference is always smaller than 180º. The reason for this is because the spacing between adjacent elements is half wavelength, and in phase this is 180º.

By looking at the results from our study, in Figure 35 the phase difference between the virtual antenna elements are plotted. As it can be seen, none of the paths that are received have an approximate 180º phase difference, which means that none of them come from the horizon. Nevertheless, we should also mention that all the paths (except from the LOS one), suffer from fading. This can also be seen in Figure 36, where the normalized amplitude is represented. Just as we have explained, we can see how the amplitude from the LOS path remains constant during the delay time while the rest do not. The reason for this is because when we defined the scenario in GCM, we set the parameters concerning the spread in angle with a low value, 1º, but by

looking at these results, we can totally see that the signals are faded and that previous value should be reconsidered.

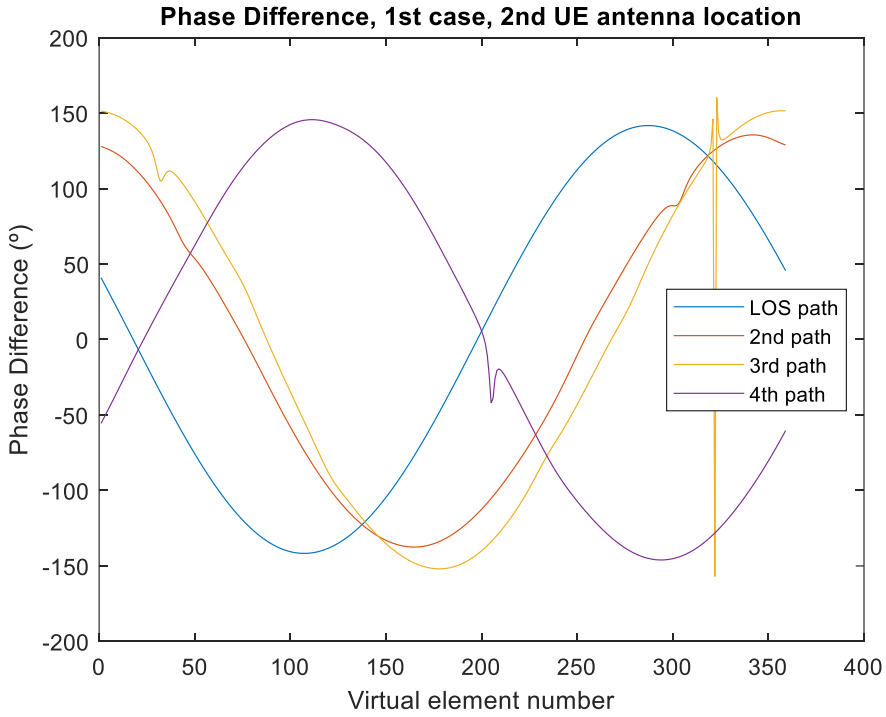

Figure 35. Phase Difference, 1st case, 2nd UE antenna location.

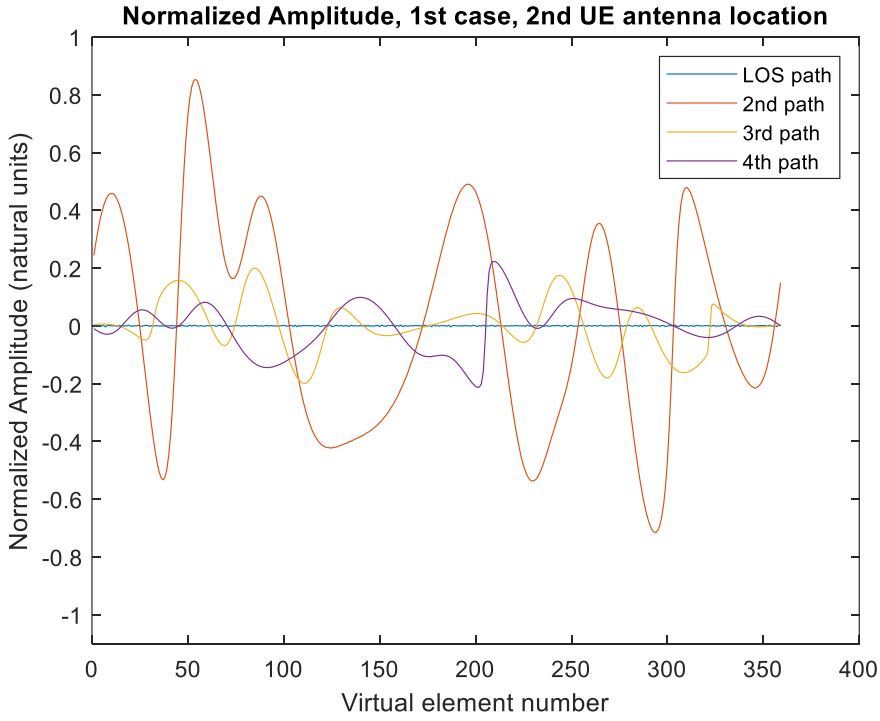

Figure 36. Normalized Amplitude, 1st case, 2nd UE antenna location.

This analysis is also done with our 2nd case scenario, and this time the antenna location chosen is the 8th one, as this one is closer to the BS and is in LOS with it. Proceeding in the same way as we have just done with the 1st case, we can see from Table 4 that when we analysed the propagation path through MATLAB, we realised that the number of paths that were received at this antenna location were also four. As we can see from Figure 37, when we plot the Channel Impulse Response obtained from GCM, for each delay sample, we can distinguish four different peaks on it. Once again, this assures that the channel is being estimated properly as these peaks correspond with the four paths which were estimated in our previous study (the first peak is at 143.5 ns, the second one is at 181 ns, the third one is at 346.5 ns, and the last one is at 350 ns). Just as in the previous case, in Figure 37 the power is also normalized respect to the LOS path which, as it can be seen from below, is the first peak. As we have already explained, this is totally reasonable as this corresponds with the definition of the scenario in GCM Tool.

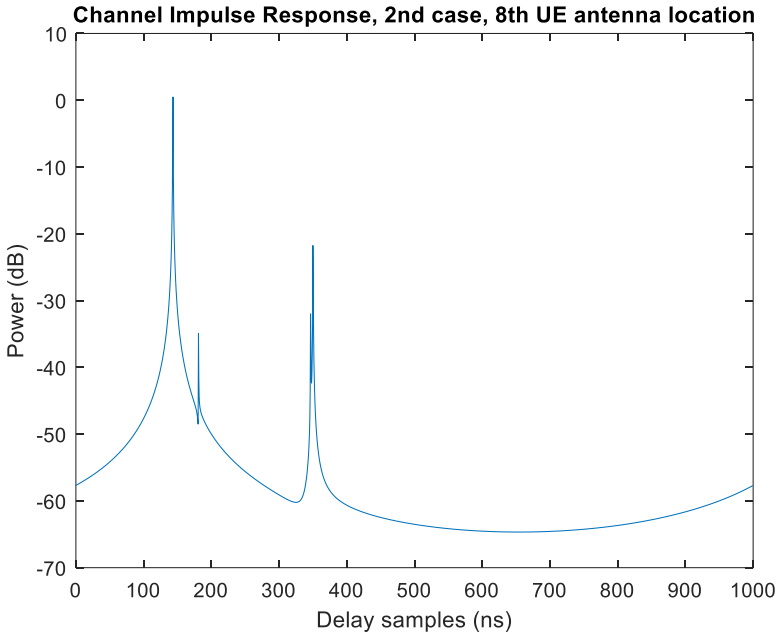

Figure 37. Channel Impulse Response, 2nd case, 8th UE location.

In this case, we can also confirm that none of the paths received at this antenna location come from the horizon as their phase difference is always below 180º. This can be seen in Figure 38. We can also check how the second, third, and fourth paths fade as in this scenario we also defined the spread in angle with 1º. Figure 39 shows the normalized amplitude and in it we can see how these paths experience a variation among the delay.

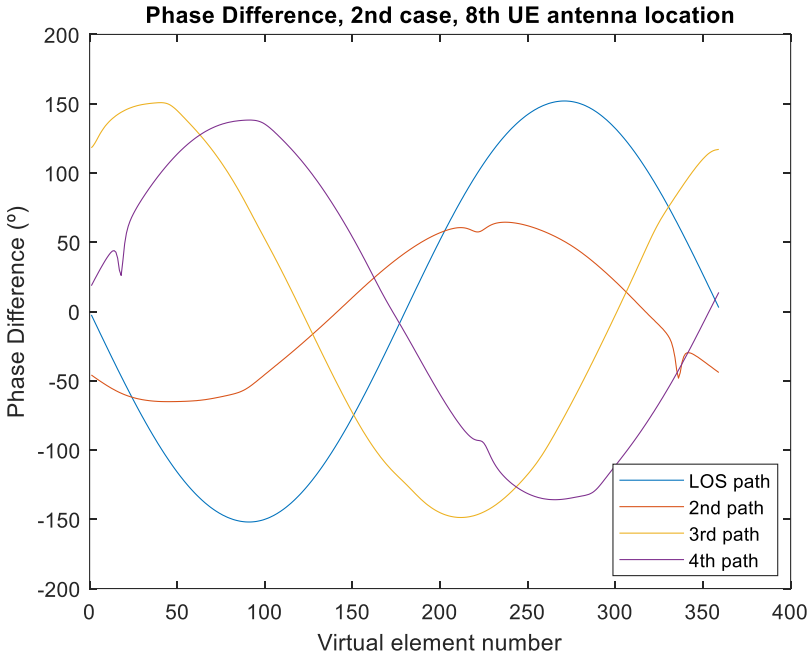

Figure 38. Phase Difference, 2nd case, 8th UE location.

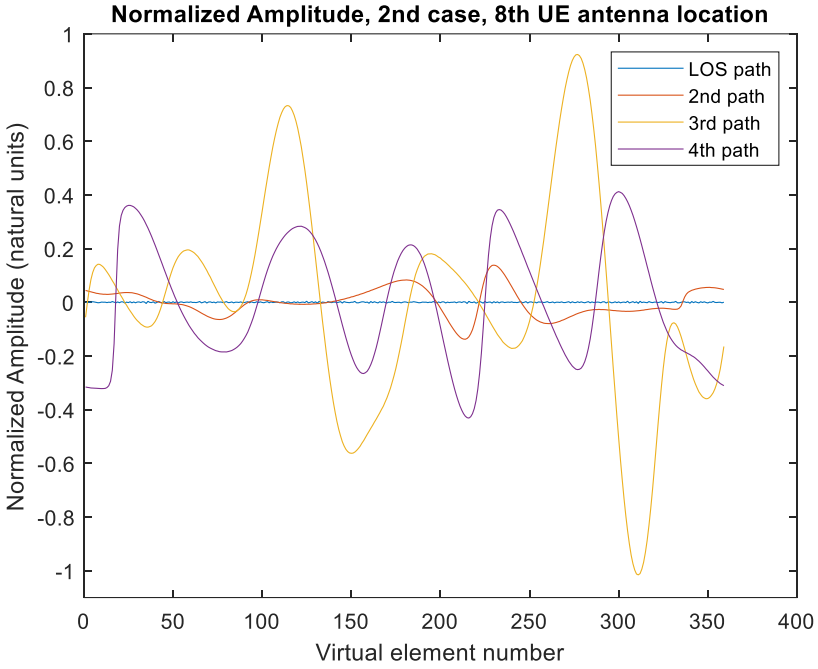

Figure 39. Normalized Amplitude, 2nd case, 8th UE antenna location.

From this analysis made for both scenarios, we can conclude that as the phase difference is always smaller than 180º, the results obtained looked reasonable, even if we could not evaluate the channel.

6 DISCUSSION

Through this work, we have been able to analyse how 5G communication channel at 29 GHz behave under different scenarios, particularly under a macrocell and a microcell environment. Due to the innovation of this communication system, the analysis of the multipath propagation channel and so its main parameters, are important as they help us to better understand this new communication network. In this way, we have analysed each scenario separately and so the signal received at each antenna. We have then collected the data from LOS and NLOS paths independently and we have then been able to draw some conclusions.

To begin with, when we started analysing the signals received at each UE location, we were able to see, for the antenna locations placed in LOS with its BS, how the first path (LOS path) was always the first one to reach the antenna, and at the same time, this path was the one that arrived with the highest intensity level. However, for some UE locations (there were one in LOS and four in NLOS condition in total for both cases), we could notice how this criterion was not always valid as the first path was not the strongest one received. The reason for this may be, especially for the NLOS conditions, that diffraction paths have shorter path lengths. As this only happened two times in the first scenario and three times in the second scenario, it can be noticed that diffractions are less often in 5G communication networks.

For both propagation conditions (LOS or NLOS), we could also see how the number of multipath components were increased in the UE positions which were surrounded by obstacles or buildings.

The delay, the azimuth, the elevation and the amplitude values, were estimated by following an estimation method that contains MUSIC and beamforming and nulling, and this allowed us to study the signal's behaviour at this frequency band. Beginning with the delay spread, we realised that due to the characteristics of the scenario and the short distance between the antennas, the results obtained in the macrocell environment (which were 27 ns in LOS and 22 ns in NLOS) were similar to the ones obtained for a microcell scenario in LOS condition (the values obtained for a microcell environment were 35 ns in LOS and 78 ns in NLOS). The results from the microcell environment satisfied better all the 3GPP requirements.

However, the azimuth spread results from both scenarios were successful as they all met the 3GPP specifications except for the macrocell environment in LOS condition. The problem we

had in this case was that we did not have too many paths arriving at the antennas so the azimuth spread was smaller than what it should had been (in the macrocell environment we got 39º in LOS and 50º in NLOS while in the microcell environment we got 50º in LOS and 46º in NLOS).

Nevertheless, when we analysed the path loss results, we applied different models regarding the propagation condition and the scenario itself. In this way, for both scenarios in LOS, we estimated the path loss values by applying the free space loss, while for the NLOS condition, we decided to apply the CI Free Space Reference Distance Model as it provides good estimations and more stable behaviour across frequencies and distances. Indeed, for the microcell scenario we also decided to implement OS model. In this part of the work, we did not achieve good results, and we also realised that there is an unknown problem, possibly related to the calibration. Indeed, we would like to highlight that the results obtained, from the first scenario, were not consistent as the path loss decreased with the distance instead of increasing.

At last, we also analysed the validity of the estimated elevation values and we realised that the results from that estimation did not correspond to the one obtained through geometry.

Finally, our last purpose was to check all these estimations by using Keysight GCM Tool. Firstly, we formulated the parameterization of the channel model by estimating the processing measurement data. Then, we specified both scenarios in GCM Tool and reconstructed the impulse response data for the corresponding channel model. Afterwards, we estimated the expected number of paths, and analysed a few example impulse responses and observed the expected number of paths. Finally, we checked the feasibility of phase behaviour of LOS path across the UCA elements.

To conclude, we would like to suggest some improvements that can be done in a way that better results are obtained. Firstly, we suggest to estimate again the elevations parameters as this issue affects the path loss values. And, secondly, it remains for further study to re-run the parameter estimation for the GCM Tool reconstructed channel data, and to compare it with the original parameter estimated directly from the measurement.

7 SUMMARY

The main goal of this thesis was to characterise and define the radio channel model at a 29 GHz frequency band for a 5G communication system.

To begin with, we have described a background theory related to the radio channel models in a way that we were able to analyse and understand the estimated parameters afterwards. In this way, we have analysed concepts such as the Geometry based Stochastic Channel Model, the Power Delay Profile, the Delay Spread, the Coherence Bandwidth and Coherence Time, the Double Directional Delay Power Spectrum, the Azimuth Spread and the Path Loss.

After that, we have described all the measurement scenarios, the measurement equipment used, and the channel estimation algorithm. This allowed us to estimate the DOA and provided us information related to the number of paths received at each UE antenna, and its delay, azimuth, elevation and amplitude values for each path.

Once we knew those parameters, we were able to analyse the pathway and characterise the radio channel by studying the delay spread, azimuth spread, path loss and elevation values. This was done for all the LOS and NLOS UE locations, and also for the macrocell and microcell environment. The MATLAB code through which we have done this analysis, not only calculates automatically those parameters, but also it compares the results obtained in our studies with the results obtained from the reference models. By doing this, through this MATLAB code we can instantaneously check the validity of the delay spread, azimuth spread and power values for any measurement cases. Indeed, this code is not only designed for our frequency band, 29 GHz, but also for any 5G high frequency band.

Afterwards, Keysight Geometric Channel Modeling Tool is used for comparing and validating the results obtained from the channel measurement, and for reconstructing the channel from our scenarios.

8 REFERENCES

[1] A. Shah, “Why We Need 5G Cellular Service,” 2019. [Online]. Available: https://www.asme.org/topics-resources/content/need-5g-cellular-service-part-2. [Accessed: 21-Mar-2020].

[2] Qualcomm, “What is 5G.” [Online]. Available: https://www.qualcomm.com/invention/5g/what-is-5g. [Accessed: 11-Apr-2020].

[3] 3GPP, “LTE,” *2020*. [Online]. Available: https://www.3gpp.org/technologies/keywords-acronyms/98-lte. [Accessed: 10-Jun-2020].

[4] B. Chen and Z. Zhong, “Geometry-based stochastic modeling for MIMO channel in high-speed mobile scenario,” *Int. J. Antennas Propag.*, vol. 2012, 2012, doi: 10.1155/2012/184682.

[5] M. Narandžić, C. Schneider, and R. Thomä, M Narandži, “Channel Models,” vol. 2007, 2007.

[6] P. Kyösti *et al.*, “Ist-4-027756 Winner II,” *Projects.Celtic-Initiative.Org*, vol. 1, no. 206, pp. 1–206, 2007.

[7] A. Goldsmith, “Wireless communications,” *Power*, vol. 150, no. 6, pp. 23–24, 2006, doi: 10.1016/b978-1-85617-921-8.00018-3.

[8] J. P. Linnartz, “Delay Spread.” [Online]. Available: http://www.wirelesscommunication.nl/reference/chaptr03/fading/delayspr.htm. [Accessed: 21-Mar-2020].

[9] Andreas F. Molisch, *Wireless Communications*, vol. 19, no. 1. 2012.

[10] J. P. Linnartz, “Coherence Bandwidth,” [Online]. Available: http://www.wirelesscommunication.nl/reference/chaptr03/cohbw/cohbw.htm. [Accessed: 21-Mar-2020].

[11] A. Jajszczyk, R. Vaughan, J. B. Andersen, and W. Dziunikowski, *Channels, Propagation and Antennas for Mobile Communications*, vol. 42, no. 6. 2004.

[12] P. Ioannides and C. A. Balanis, “Uniform circular arrays for smart antennas,” *IEEE Antennas Propag. Mag.*, vol. 47, no. 4, pp. 192–206, 2005, doi: 10.1109/MAP.2005.1589932.

[13] W. Fan, F. Zhang, and Z. Wang, “Over-the-Air Testing of 5G Communication Systems: Validation of the Test Environment in Simple-Sectored Multiprobe Anechoic Chamber

Setups," *IEEE Antennas Propag. Mag.*, pp. 0–0, 2019, doi: 10.1109/map.2019.2943305.

[14] Merriam-Webster, "Snell's Law." [Online]. Available: https://www.merriam-webster.com/dictionary/Snell%27s law. [Accessed: 10-Apr-2020].

[15] 3GPP, "Specification 38.901." 2019.

[16] S. Sun *et al.*, "Propagation Path Loss Models for 5G Urban Micro- and Macro-Cellular Scenarios," Nov. 2015, doi: 10.1109/VTCSpring.2016.7504435.

[17] S. Sun, G. R. MacCartney, and T. S. Rappaport, "Millimeter-wave distance-dependent large-scale propagation measurements and path loss models for outdoor and indoor 5G systems," *2016 10th Eur. Conf. Antennas Propagation, EuCAP 2016*, no. EuCAP, 2016, doi: 10.1109/EuCAP.2016.7481506.

[18] P. Theodore Rappaport and S. Shu Sun, "Investigation of prediction accuracy, sensitivity, and parameter stability of large-scale propagation path loss models from 500 MHz to 100 GHz Presentation for NTIA," 2016.

[19] S. S. Zhekov, A. Tatomirescu, and G. F. Pedersen, "Antenna for Ultrawideband Channel Sounding," *IEEE Antennas Wirel. Propag. Lett.*, vol. 16, pp. 692–695, 2017, doi: 10.1109/LAWP.2016.2600245.

[20] Keysight Technologies, "PROPSIM GCM 5G Tool. Installing and using the software. User Guide," p. 111, 2020.

9 APPENDICES

Appendix 1 1st case results.

Appendix 2 2nd case results.

Appendix 3 MATLAB code.

Appendix 4 Path estimation.

Appendix 5 Parameters' values for the 1st case.

Appendix 6 Parameters' values for the 2nd case.

Appendix 1 1st case scenario.

In this section all the results from the measurement data for the 1st case are plotted.

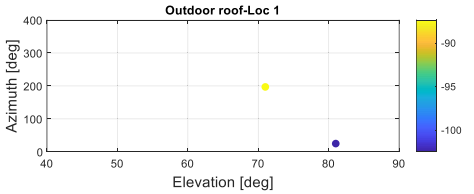

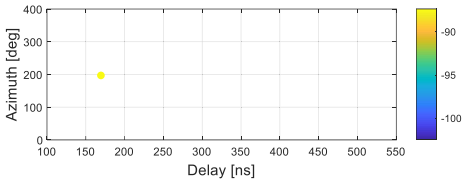

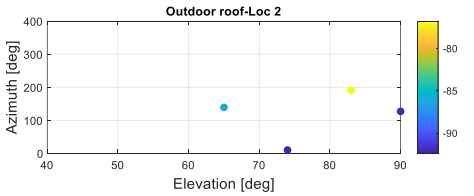

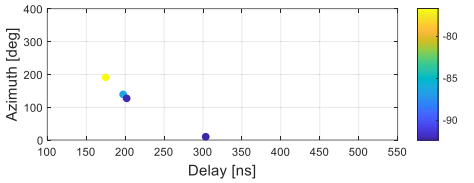

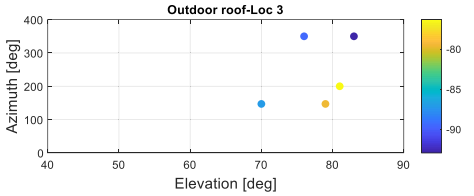

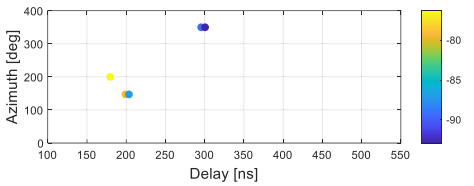

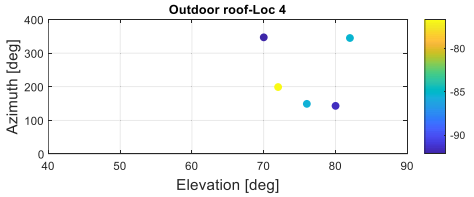

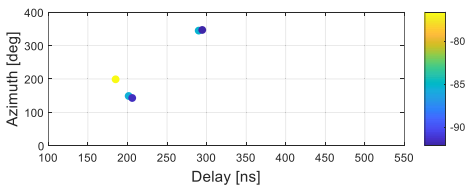

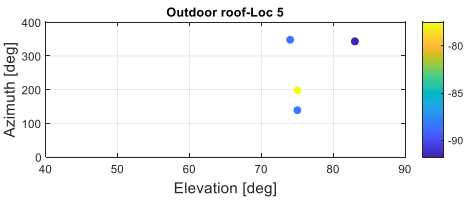

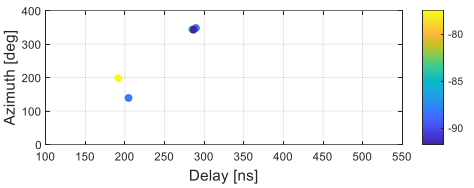

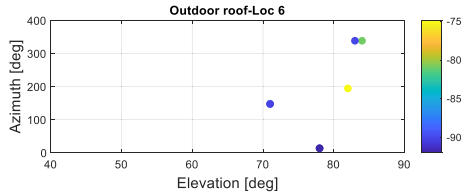

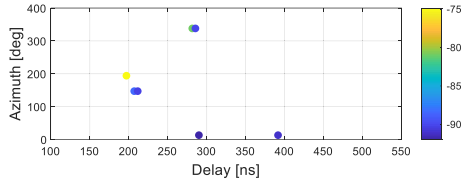

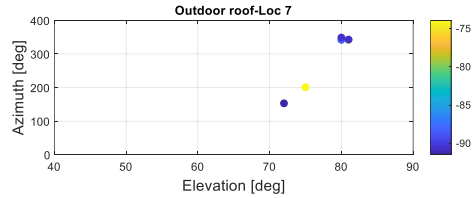

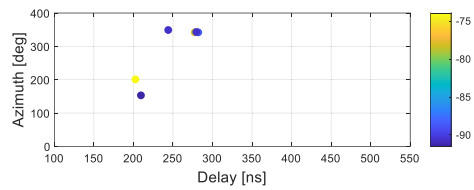

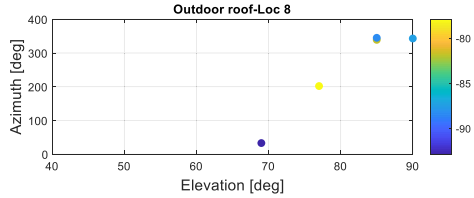

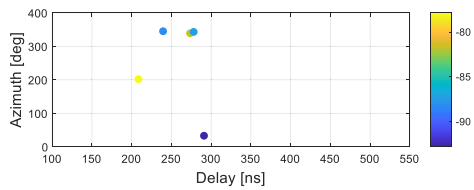

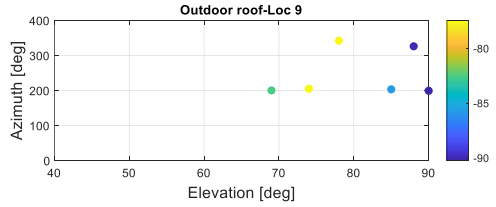
Outdoor roof-Loc 9
Azimuth [deg]
Elevation [deg]

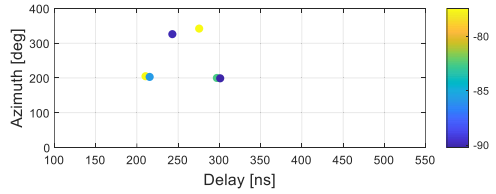
Azimuth [deg]
Delay [ns]

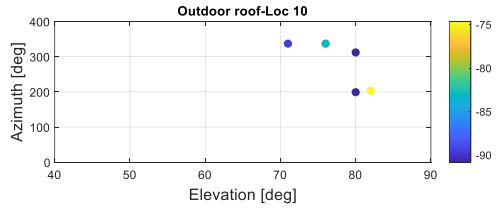
Outdoor roof-Loc 10
Azimuth [deg]
Elevation [deg]

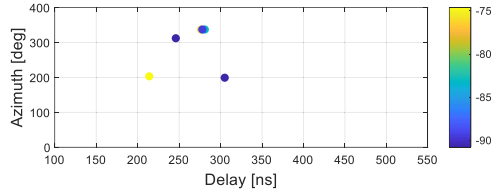
Azimuth [deg]
Delay [ns]

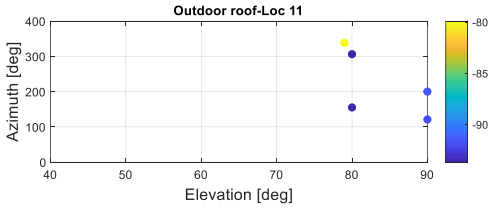
Outdoor roof-Loc 11
Azimuth [deg]
Elevation [deg]

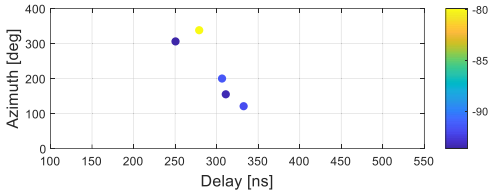
Azimuth [deg]
Delay [ns]

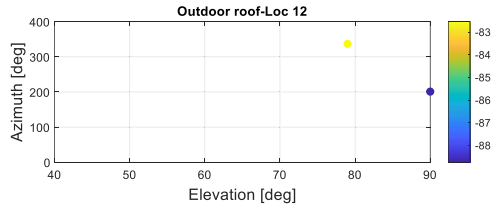
Outdoor roof-Loc 12
Azimuth [deg]
Elevation [deg]

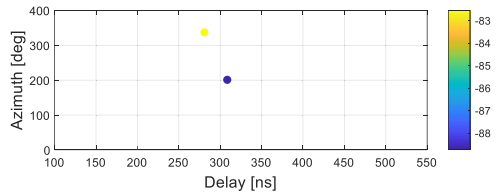
Azimuth [deg]
Delay [ns]

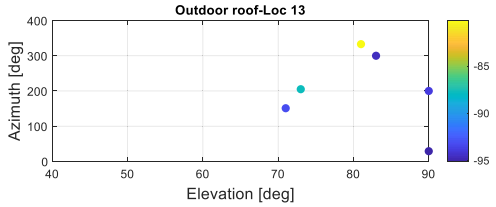
Outdoor roof-Loc 13
Azimuth [deg]
Elevation [deg]

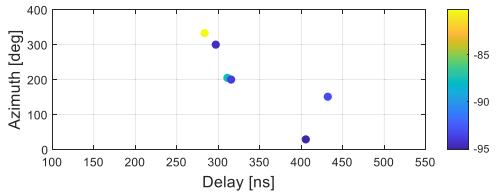
Azimuth [deg]
Delay [ns]

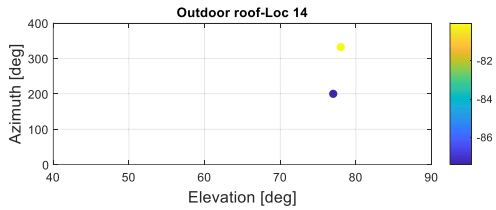
Outdoor roof-Loc 14
Azimuth [deg]
Elevation [deg]

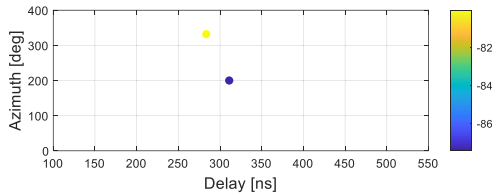
Azimuth [deg]
Delay [ns]

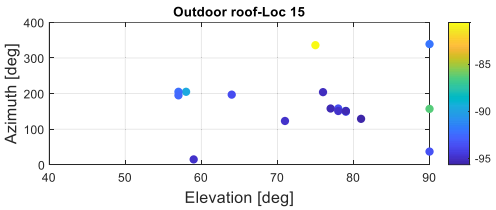
Outdoor roof-Loc 15
Azimuth [deg]
Elevation [deg]

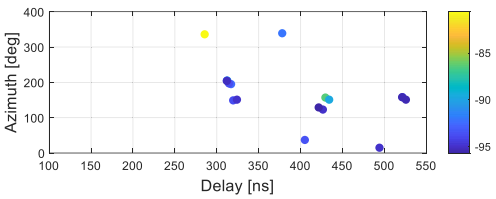
Azimuth [deg]
Delay [ns]

Appendix 2 2nd case scenario.

In this section all the results from the measurement data for the 2nd case are plotted.

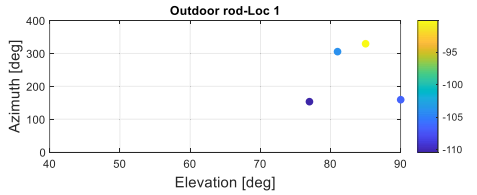

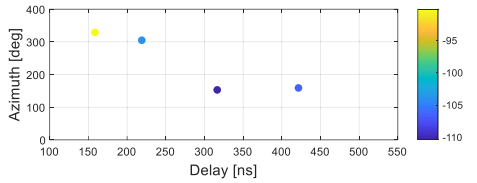

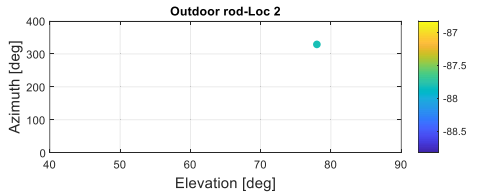

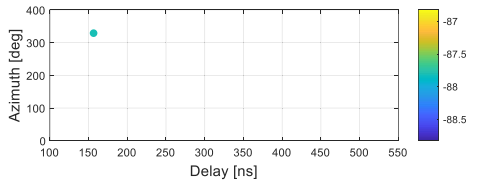

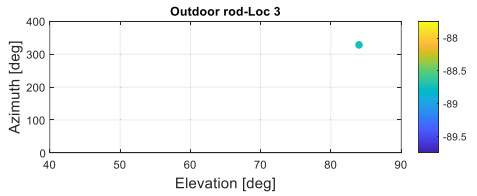

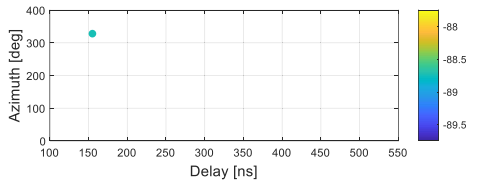

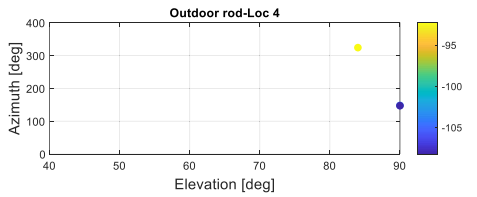

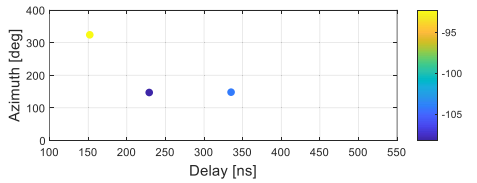

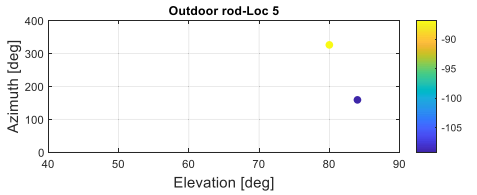

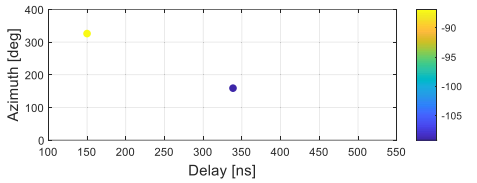

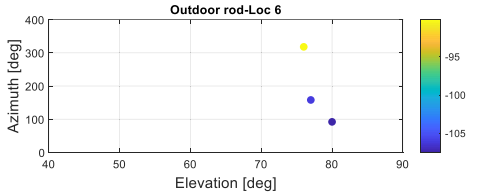

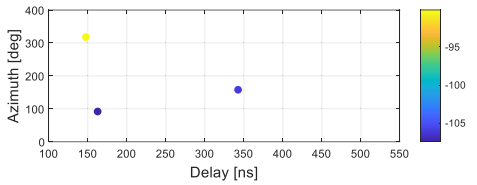

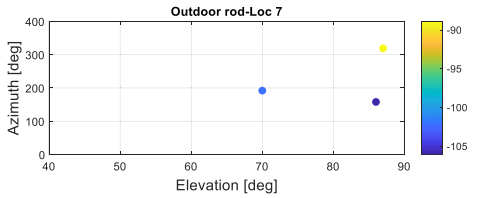

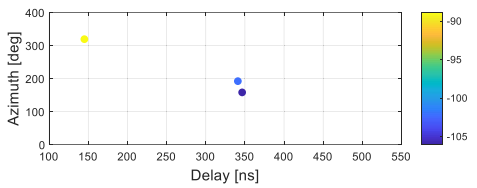

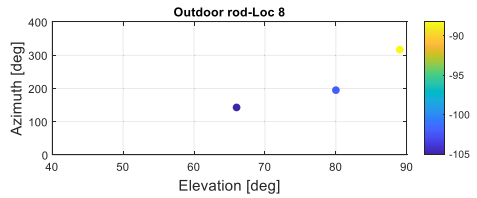

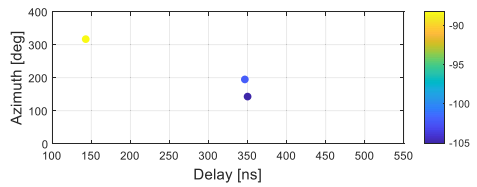

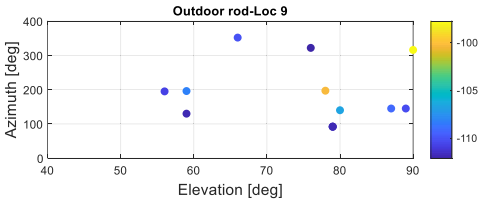
Outdoor rod-Loc 9
Azimuth [deg]
Elevation [deg]

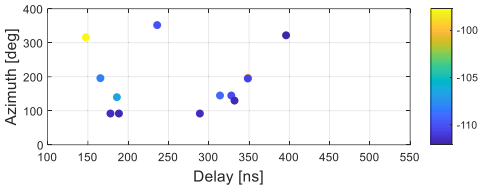
Azimuth [deg]
Delay [ns]

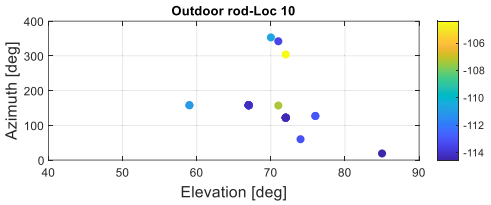
Outdoor rod-Loc 10
Azimuth [deg]
Elevation [deg]

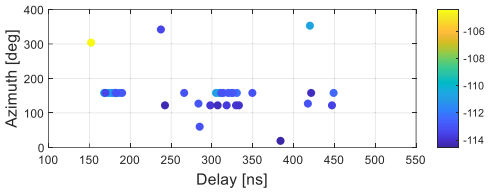
Azimuth [deg]
Delay [ns]

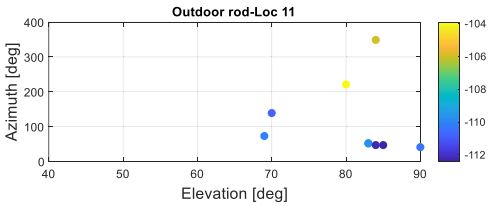
Outdoor rod-Loc 11
Azimuth [deg]
Elevation [deg]

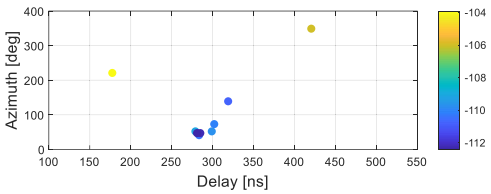
Azimuth [deg]
Delay [ns]

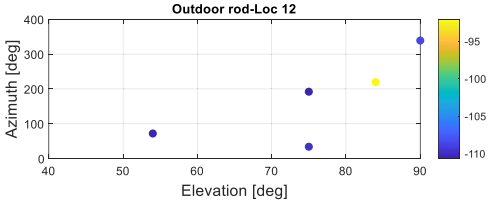
Outdoor rod-Loc 12
Azimuth [deg]
Elevation [deg]

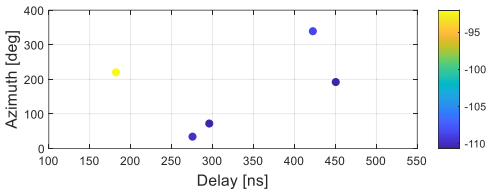
Azimuth [deg]
Delay [ns]

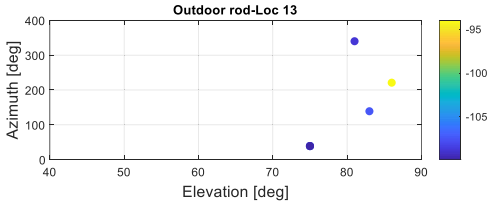
Outdoor rod-Loc 13
Azimuth [deg]
Elevation [deg]

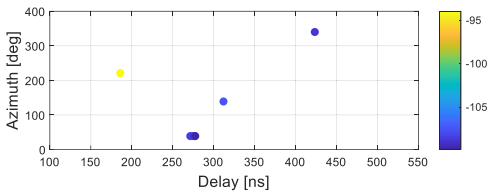
Azimuth [deg]
Delay [ns]

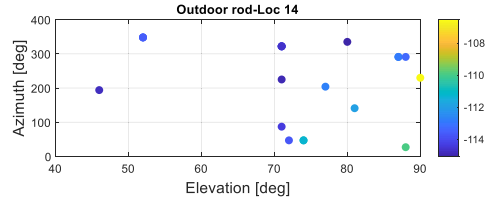
Outdoor rod-Loc 14
Azimuth [deg]
Elevation [deg]

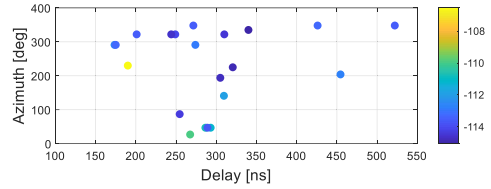
Azimuth [deg]
Delay [ns]

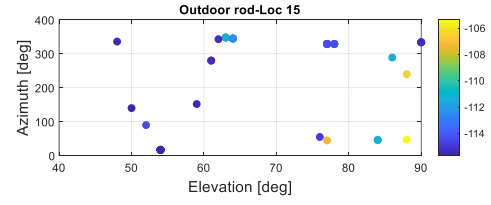
Outdoor rod-Loc 15
Azimuth [deg]
Elevation [deg]

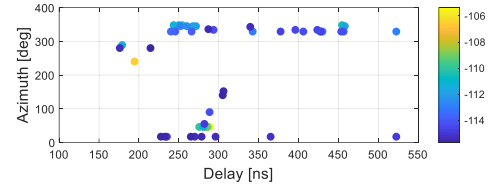
Azimuth [deg]
Delay [ns]

Appendix 3 MATLAB code.

In this section the MATLAB code implemented for this thesis is shown.

```
% Author: Belén González Lozano,
% Master Thesis, University of Oulu, 2019/2020

% Through this MATLAB code, it is calculated the delay and the angular spread, and
the average path loss. Those results are then compared with the reference values so
it can be seen its accuracy.

% Structure of the loaded file:
% est_para( PARAMETER , RESULTS(1-50) , ANTENNA LOCATION NUMBER )

% Parameters:
% est_para(1,:,i) is the ELEVATION value (rad) for the antenna i
% est_para(2,:,i) is the AZIMUTH value (rad) for the antenna i
% est_para(3,:,i) is the DELAY value (s) for the antenna i
% est_para(4,:,i) is the AMPLITUDE value (natural units) for the antenna i


clear;
clc;
close all;

% The file should contain ELEVATION, AZIMUTH, DELAY and AMPLITUDE values
load('C:\Users\belen\Desktop\TFM\Matlab\code\TOP\ToOulu\Outdoor_roof\est_para.mat')
; %file with the elevation, azimuth, delay and amplitude values

% Input parameters:
macro = 1;                      % macro = 1 means macrocell environment, macro = 0
means microcell environment
fc = 29;                        % Carrier frequency, GHz
c = 299792458;                  % Speed of light, m/s
lambda = c /(fc*1e9);           % Wavelength, m
Dynamic_Range = -30;            % Threshold, dB
N = 15;                         % Number of rx antennas (this code is for only 1
transmitter antenna)
N_LOS = 10;                     % Number of rx antennas in LOS condition
N_NLOS = 5;                     % Number of rx antennas in NLOS condition
P = 50;                         % Maximum amount of paths received per antenna
distance_LOS = [50.81 52.46 53.81 55.46 57.41 59.06 60.71 62.51 63.11 64.16];   %
Vector 1xN with the distances (in metres) between the tx and rx antennas
```

```
distance_NLOS = [75.10 84.24 84.99 84.99 85.59];           % meters from the delay

% distance_roof_LOS_d1 = [50.46 52.01 53.57 55.53 57.10 59.07 60.65 63.04 64.63
65.43];                                                    % meters from the map
% distance_roof_LOS_d2 = [50.81 52.46 53.81 55.46 57.41 59.06 60.71 62.51 63.11
64.16];                                                    % meters from the delay
% distance_roof_NLOS_d2 = [75.10 84.24 84.99 84.99 85.59]; % meters from the delay
%
% distance_rod_LOS_d1 = [49.29 48.46 47.62 46.79 45.96 45.12 44.29 43.45]; % meters
from the map
% distance_rod_LOS_d2 = [47.52 46.92 46.47 45.57 44.97 44.22 43.47 42.87]; % meters
from the delay
% distance_rod_NLOS_d2 = [44.22 45.57 53.21 54.56 55.76 52.01 52.76];    % meters
from the delay


% % Output parameters:
% S_d*1e9;                % Delay Spread, ns
% rad2deg(S_a);           % Azimuth Spread, degrees
% path_loss_total_abs;    % Path loss values



% Calculations:


% DELAY SPREAD CALCULATION %

a=zeros(1,P);
b=zeros(1,P);
c=zeros(1,P);
for i=1:N
    p_h = abs(squeeze(est_para(4,:,i))).^2; % vector with the power of all the
different paths (1x50)
    delay = squeeze(est_para(3,:,i)); % vector with the delay from all the
different paths (1x50)
    max_power = max(20*log10(squeeze(est_para(4,:,i)))); % result with the highest
power
    for k=1:P
        if ( max_power + Dynamic_Range < 20*log10(squeeze(est_para(4,k,i))) )
            a(k) = p_h(k).*delay(k);
            b(k) = p_h(k).*(delay(k)).^2;
            c(k) = p_h(k);
        else
            a(k) = 0;
```

```
            b(k) = 0;
            c(k) = 0;
        end
    end
    p_m(i) = sum(c); % vector with the total power for each antenna location
    T_m(i) = sum(a)/p_m(i);
    S_d(i) = sqrt(sum(b)/p_m(i) - (T_m(i))^2);
end
S_d*1e9;


% Reference values: 3GPP TR 38.901
if macro == 1
    S_d_Uma_LOS = zeros(1,N_LOS);
    S_d_Uma_NLOS = zeros(1,N_NLOS);
    for i = 1:N_LOS
        S_d_Uma_LOS(i) = (10^(-6.955 - 0.0963*log10(fc)))*1e9; % rms Delay Spread
LOS (ns), macrocell environment
    end
    for i = 1:N_NLOS
        S_d_Uma_NLOS(i) = (10^(-6.28 - 0.204*log10(fc)))*1e9; % rms Delay Spread
NLOS (ns), macrocell environment
    end
    S_d_ref=[S_d_Uma_LOS S_d_Uma_NLOS];
else
    S_d_Umi_LOS = zeros(1,N_LOS);
    S_d_Umi_NLOS = zeros(1,N_NLOS);
    for i = 1:N_LOS
        S_d_Umi_LOS(i) = (10^(-0.24*log10(1+fc) - 7.14))*1e9; % rms Delay Spread
LOS (ns, microcell environment)    (log scale, but no dB!)
    end
    for i = 1:N_NLOS
        S_d_Umi_NLOS(i) = (10^(-0.24*log10(1+fc) - 6.83))*1e9; % rms Delay Spread
NLOS (ns), microcell environment
    end
    S_d_ref=[S_d_Umi_LOS S_d_Umi_NLOS];
end


% Plots
figure(1);
plot(S_d*1e9, '-o')
hold on
plot(S_d_ref, '--r')
hold off
```

```
xlabel('Antenna location number');
ylabel('Delay Spread [ns]');
if macro ==1
    title(['Delay Spread comparison in a macrocell environment, @ ',num2str(fc),'
GHz'])
else
    title(['Delay Spread comparison in a microcell environment, @ ',num2str(fc),'
GHz'])
end
legend({'Delay Spread','Reference values'},'Location','northwest');
grid;
xlim([0 (N+1)]);



% AZIMUTH SPREAD %


APS=zeros(1,P);
d=zeros(1,P);
e=zeros(1,P);
for i=1:N
    d = squeeze(est_para(2,:,i)); % azimuth values
    max_power = max(20*log10(squeeze(est_para(4,:,i)))); % result with the highest
power
    for k=1:P
        if ( max_power + Dynamic_Range < 20*log10(squeeze(est_para(4,k,i))) )
           APS(k) = abs(d(k)).^2;
        else
           APS(k) = 0;
        end
    e(k) = exp(1j.*d(k)) .* APS(k);
    end
    nu(i) = sum(e) / sum(APS);
    S_a(i) = sqrt( sum( (abs( exp(1j.*d) - nu(i) ).^2) .* APS ) / sum(APS) );
end
rad2deg(S_a);


% Reference: 3GPP TR 38.901
if macro == 1
    S_a_Uma_LOS = zeros(1,N_LOS);
    S_a_Uma_NLOS = zeros(1,N_NLOS);
    for i = 1:N_LOS
        S_a_Uma_LOS(i) = 10^(1.81); % AOA, Azimuth Of Arrival LOS (°)
```

```
    end
    for i = 1:N_NLOS
        S_a_Uma_NLOS(i) = 10^(2.08 - 0.27*log10(fc)); % AOA, Azimuth Of Arrival
NLOS (°)
    end
    S_a_ref=[S_a_Uma_LOS S_a_Uma_NLOS];
else
    S_a_Umi_LOS = zeros(1,N_LOS);
    S_a_Umi_NLOS = zeros(1,N_NLOS);
    for i = 1:N_LOS
        S_a_Umi_LOS(i) = 10^(-0.08*log10(1+fc) + 1.73); % AOA, Azimuth Of Arrival
LOS (°)
    end
    for i = 1:N_NLOS
        S_a_Umi_NLOS(i) = 10^(-0.08*log10(1+fc) + 1.81); % AOA, Azimuth Of Arrival
NLOS (°)
    end
    S_a_ref=[S_a_Umi_LOS S_a_Umi_NLOS];
end


% Plots
figure(2);
plot(rad2deg(S_a), '-o')
hold on
plot(S_a_ref, '--r')
hold off
xlabel('Antenna location number');
ylabel('Azimuth Spread [ ° ]');
if macro ==1
    title(['Azimuth Spread comparison in a macrocell environment, @ ',num2str(fc),'
GHz'])
else
    title(['Azimuth Spread comparison in a microcell environment, @ ',num2str(fc),'
GHz'])
end
legend({'Azimuth Spread','Reference values'},'Location','southwest');
grid;
xlim([0 (N+1)]);


% PATH LOSS %

% Calculated as the sum in natural units of the amplitude values
```

```
path_loss_total = zeros(1,N);
for i=1:N
    path_loss = zeros(1,P);
    max_power = max(20*log10(squeeze(est_para(4,:,i)))); % result with the highest
power
    for k=1:50
        if ( max_power + Dynamic_Range < 20*log10(squeeze(est_para(4,k,i))) )
           path_loss(k) = squeeze(est_para(4,k,i)); % natural units!!
        else
           path_loss(k) = 0;
        end
    end
    path_loss_total(i) = sum(path_loss.^2); % sum in natural units
end
path_loss_total_abs=abs(10*log10(path_loss_total));


% Reference value:
% LOS condition
PL_LOS = fspl(distance_LOS,lambda);

% NLOS condition, CI model
% Regarding the microcell, the Open Street Model is used (street canyon is not
applicable in our case)
if macro == 1
    PL_NLOS_CI = 32.4 + 30*log10(distance_NLOS) + 20*log10(fc); % sigma = 6.8 dB
else
    PL_NLOS_CI = 32.4 + 29*log10(distance_NLOS) + 20*log10(fc); % sigma = 7.1 dB
Open Street Model
end

% % Regarding the microcell, Street Canyon Model (in case it is applicable)
% if macro == 1
%     PL_NLOS_CI = 32.4 + 30*log10(distance_NLOS) + 20*log10(fc); % sigma = 6.8 dB
% else
%     PL_NLOS_CI = 32.4 + 32*log10(distance_NLOS) + 20*log10(fc); % sigma = 8.1 dB
Street Canyon Model
% end

PL_ref=[PL_LOS PL_NLOS_CI]; % Vector with the reference path loss for LOS and NLOS


% Plots
figure(3);
plot(path_loss_total_abs, '-o')
```

```
hold on
plot(PL_ref, '--r')
hold off
xlabel('Antenna location number');
ylabel('Path loss (dB)');
if macro == 1
    title(['Path loss comparison in a macrocell environment, @ ',num2str(fc),'
GHz'])
else
    title(['Path loss comparison in a microcell environment, @ ',num2str(fc),'
GHz'])
end
legend({'Path loss','Reference values'},'Location','northwest');
grid;
xlim([0 (N+1)]);
y_min=(min(path_loss_total_abs)-10);
y_max=(max(PL_ref))+10;
ylim([y_min, y_max]);


% VIEW OF THE PATHS %

% Number of paths:

final_e_k = zeros(1,N);
for i=1:N
    e_k = 0;
    final_paths_i = zeros(1,P);
    max_value_i = max(20*log10(squeeze(est_para(4,:,i)))); % result with the
highest power
    for k=1:P
        if ( max_value_i + Dynamic_Range < 20*log10(squeeze(est_para(4,k,i))) )
            final_paths_i(k) = squeeze(est_para(4,k,i));
            e_k(k) = 1;
        else
            final_paths_i(k) = 0;
            e_k(k) = 0;
        end
    end
    final_paths_i;
    final_e_k(i) = sum(e_k);
end
final_e_k; % Number of paths at each UE location

% This is done for knowing the accurate values so we can plot the results better
```

```
all_delay_values = zeros(1,sum(final_e_k));
all_power_values = zeros(1,sum(final_e_k));
var=1;
if var <= sum(final_e_k)
    for i=1:N
        for k=1:final_e_k(i)
            all_delay_values(var) = squeeze(est_para(3,k,i));
            all_power_values(var) = squeeze(est_para(4,k,i));
            var=var+1;
        end
    end
else
    return;
end
min_delay = min(all_delay_values*1e9);
max_delay = max(all_delay_values*1e9);
min_power = min(20*log10(all_power_values));
max_power = max(20*log10(all_power_values));
cte = 10; % this value is for plotting in a wider range, see axis (line 320)

for i=1:N
    x1 = linspace(1,N,N);
    max_value = max(20*log10(squeeze(est_para(4,:,i))));
    for k=1:50
        if ( max_value + Dynamic_Range < 20*log10(squeeze(est_para(4,k,i))) )
           z1(k) = squeeze(est_para(4,k,i)); % power
           y1(k) = squeeze(est_para(3,k,i))*1e9; % delay
        else
           z1(k) = 0; % power
           y1(k) = 0; % delay
        end
    end
    final_y1 = zeros(1,final_e_k(i));
    final_z1 = zeros(1,final_e_k(i));
    for k = 1:final_e_k(i)
        final_y1(k) = y1(k);
        final_z1(k) = z1(k);
    end
    w1 = [final_y1',20*log10(final_z1)']; % delay and power

    figure(4)
    plot3(zeros(1,final_e_k(i))+x1(i), w1(:,1), zeros(length(w1),1),'*r')
    grid
    axis([0,16,min_delay-cte,max_delay+cte,min_power-cte,max_power+cte]);
```

```
    stem3(zeros(1,final_e_k(i))+x1(i),w1(:,1),w1(:,2),'^','fill','BaseValue',
min_power-cte)

    hold on

    xlabel('x: antenna location number');
    ylabel('y: delay [ns]');
    zlabel('z: power (dB)');
    if(macro==1)
        title('Macrocell environment');
    else
        title('Microcell environment');
    end
end
hold off


% Results obtained:
fprintf('Delay Spread:\n');
fprintf('Values obtained (ns):\n');
fprintf('%.2f ', S_d*1e9);
fprintf('\n');
fprintf('Reference values (ns):\n');
fprintf('%.2f ', S_d_ref);
fprintf('\n');
fprintf('\n');
fprintf('Azimuth Spread:\n');
fprintf('Values obtained (°):\n');
fprintf('%.2f ', rad2deg(S_a));
fprintf('\n');
fprintf('Reference values (°):\n');
fprintf('%.2f ', S_a_ref);
fprintf('\n');
fprintf('\n');
fprintf('Path loss:\n');
fprintf('Values obtained (dB):\n');
fprintf('%.2f ', path_loss_total_abs);
fprintf('\n');
fprintf('Reference values (dB):\n');
fprintf('%.2f ', PL_ref);
fprintf('\n');
fprintf('\n');
```

Appendix 4 Path estimation.

In this excel page we can see the way the path estimation was calculated as we discussed in the Section 4.1.1

higest power										
c (m/ns)	0,30									
1st case										
Location , nº of the path	Elevation (º)	Azimuth (º)	Delay (ns)	Distance on the map (cm) [d1', d1''...]				Distance (m) [d1]	Distance from the delay [d2]	Comments
1,1	71	197	169,5	5,6				50,85	50,81	ok
1,2	81	25	550,5	6,5	2,5	6,5	4	166,35	165,04	ok, Snell's law ok too
3,1	81	200	179,5	5,9				53,16	53,81	ok
3,2	79	147	199	6	0,9			61,45	59,66	ok, Snell's law ok too
7,1	75	201	202,5	6,9				60,97	60,71	ok
7,4	81	342	277,5	8,1	1,55			83,45	83,19	ok, Snell's law ok too
8,1	77	202	208,5	7,2				63,34	62,51	ok
8,2	85	345	239,5	8	1			78,06	71,80	ok, Snell's law ok too
2nd case										
Location , nº of the path	Elevation (º)	Azimuth (º)	Delay (ns)	Distance on the map (cm) [d1', d1''...]				Distance (m) [d1]	Distance from the delay [d2]	Comments
1,1	85	329	158,5	5,9				49,34	47,52	ok
1,4	90	159	421,5	8,3	2,7	2,7		114,43	126,36	I have not found the exact path for this ray
				8,6	2,5	2,7		115,26		
5,1	80	326	150	5,5				46,01	44,97	ok
6,1	76	318	147,5	5,4				45,18	44,22	ok
6,3	77	158	342,5	6,5	2,2	2,5	0,7	99,42	102,68	ok, Snell's law ok too
8,1	89	317	143	5,2				43,51	42,87	ok
8,3	66	143	350	8,5	2,3	1,2		100,24	104,93	ok, Snell's law ok too
11,1	80	221	177,5	5,6	0,8			53,52	53,21	ok, Snell's law ok too

Appendix 5 Parameters' values for the 1st case.

In this appendix it is shown all the estimated parameters' values used for Keysight's GCM Tool, for the first case.

	This colour represents the first path and/or reference path
	This colour represents the paths stronger than the reference path

MS number	Power multiplied by	Estimated power	Power for GCM	Estimated delay	Delay for GCM	Estimated AoA	Adaptation for GCM	AoA obtained from GCM	Estimated EoA	Adaptation for GCM	EoA obtained from GCM
1	1.0e-04	0,2671	0	169,5	169,00	197	-107	-107,43	71	19	22,03
		0,0085	-29,95	550,5	381,5	25	65		81	9	
2	1.0e-04	0,8042	0	175,0	175,38	191	-101	-106,11	83	7	21,18
		0,2437	-10,37	197,5	22,1	139	-49		65	25	
		0,0438	-25,28	202,0	26,6	127	-37		90	0	
		0,0541	-23,44	303,5	128,1	10	80		74	16	
3	1.0e-03	0,1244	0,00	179,5	178,88	200	-110	-109,16	81	9	20,75
		0,0818	-3,64	199,0	20,1	147	-57		79	11	
		0,0282	-12,89	203,5	24,6	147	-57		70	20	
		0,0213	-15,33	295,5	116,6	350	-100		76	14	
		0,0071	-24,87	300,5	121,6	350	-100		83	7	
4	1.0e-04 *	0,9872	0,00	185,0	185,67	199	-109	-109,19	72	18	19,96
		0,3195	-9,80	201,5	15,8	149	-59		76	14	
		0,5164	-5,63	290,0	104,3	345	-105		82	8	
		0,1348	-17,29	206,0	20,3	143	-53		80	10	
		0,0886	-20,94	294,5	108,8	347	-103		70	20	
5	1.0e-04 *	0,6973	0,00	191,5	192,24	198	-108	-108,98	75	15	19,25
		0,3946	-4,95	285,0	92,8	344	-106		83	7	
		0,2156	-10,20	204,5	12,3	139	-49		75	15	
		0,136	-14,20	289,5	97,3	348	-102		74	16	
		0,0579	-21,61	286,5	94,3	343	-107		83	7	
6	1.0e-03	0,1308	0,00	197,0	197,68	194	-104	-107,63	82	8	18,7
		0,0595	-6,84	281,5	83,8	338	-112		84	6	
		0,0165	-17,98	207,0	9,3	147	-57		71	19	
		0,02	-16,31	285,5	87,8	338	-112		83	7	
		0,0095	-22,78	211,5	13,8	147	-57		71	19	
		0,0048	-28,71	391,5	193,8	13	77		78	12	
		0,0047	-28,89	290,0	92,3	13	77		78	12	
7	1.0e-03	0,1748	0,00	202,5	202,50	201	-111	-111,05	75	15	18,24
		0,0898	-5,79	277,5	75,0	342	-108		81	9	
		0,0298	-15,37	282,0	79,5	342	-108		80	10	
		0,0098	-25,03	279,5	77,0	343	-107		81	9	
		0,0156	-20,99	244,0	41,5	349	-101		80	10	
		0,0175	-19,99	209,5	7,0	153	-63		72	18	
8	1.0e-03	0,108	0,00	208,5	208,01	202	-112	-111,53	77	13	17,74
		0,039	-8,85	273,5	65,5	339	-111		85	5	
		0,0165	-16,32	278,0	70,0	343	-107		90	0	
		0,0157	-16,75	239,5	31,5	345	-105		85	5	
		0,0043	-28,00	291,0	83,0	33	57		69	21	
9	1.0e-03	0,1249	2,79	275,5	64,3	342	-108		78	12	
		0,0906	0,00	210,5	211,2	205	-115	-113,62	74	16	17,46
		0,0325	-8,90	297,0	85,8	200	-110		69	21	
		0,0256	-10,98	215,5	4,3	203	-113		85	5	
		0,0093	-19,77	301,0	89,8	199	-109		90	0	
		0,0212	-12,62	243,0	31,8	326	-124		88	2	
10	1.0e-03	0,1733	0,00	214,0	214,55	203	-113	-112,99	82	8	17,18
		0,1139	-3,65	276,5	62,0	337	-113		76	14	
		0,0426	-12,19	281,0	66,5	337	-113		76	14	
		0,0217	-18,05	278,0	63,5	337	-113		71	19	
		0,0208	-18,41	246,0	31,5	312	-138		80	10	
		0,014	-21,85	305,0	90,5	199	-109		80	10	
11	1.0e-04 *	0,978	19,80	279,0	28,5	338	-112		79	11	
		0,2693	8,60	306,5	56,0	200	-110		90	0	
		0,1227	1,77	332,5	82,0	121	-31		90	0	
		0,0482	-6,35	311,0	60,5	155	-65		80	10	
		0,1001	0,00	250,5	0,0	306	-144		80	10	

12	1.0e-04 *	0,9536	0,00	281,0	0,0	337	-113		79	11
		0,1414	-16,58	308,5	27,5	201	-111		90	0
13	1.0e-04 *	0,6768	0,00	283,5	0,0	333	-117		81	9
		0,3306	-6,22	311,0	27,5	205	-115		73	17
		0,0369	-25,27	432,0	148,5	151	-61		71	19
		0,1064	-16,07	315,5	32,0	200	-110		90	0
		0,0274	-27,85	297,0	13,5	300	-150		83	7
		0,0415	-24,25	405,5	122,0	29	61		90	0
14	1.0e-04 *	0,8999	0,00	283,5	0,0	332	-118		78	12
		0,3428	-8,38	311,0	27,5	200	-110		77	13
15	1.0e-04 *	0,3839	0,00	285,5	0,0	336	-114		75	15
		0,3127	-1,78	429,5	144,0	157	-67		90	0
		0,0794	-13,69	312,5	27,0	205	-115		58	32
		0,0974	-11,91	434,0	148,5	151	-61		79	11
		0,0288	-22,50	312,0	26,5	205	-115		57	33
		0,0599	-16,14	378,0	92,5	339	-111		90	0
		0,0543	-16,99	317,0	31,5	195	-105		57	33
		0,0244	-23,94	314,5	29,0	197	-107		64	26
		0,0448	-18,66	319,5	34,0	149	-59		79	11
		0,0518	-17,40	521,5	236,0	158	-68		78	12
		0,0422	-19,18	405,0	119,5	37	53		90	0
		0,0378	-20,13	324,0	38,5	151	-61		78	12
		0,0142	-28,64	494,0	208,5	15	75		59	31
		0,0181	-26,53	525,5	240,0	151	-61		79	11
		0,0135	-29,08	426,5	141,0	123	-33		71	19

Appendix 6 Parameters' values for the 2nd case.

In this appendix it is shown all the estimated parameters' values used for Keysight's GCM Tool, for the second case.

	This colour represents the first path and/or reference path
	This colour represents the paths stronger than the reference path

MS number	Power multiplied by	Estimated power	Power for GCM	Estimated delay	Delay for GCM	Estimated AoA	Adaptation for GCM	AoA obtained from GCM	Estimated EoA	Adaptation for GCM	EoA obtained from GCM
1	1.0e-04	0,3113	0	158,5	158,11	329	121	120,87	85	5	2,42
		0,0646	-13,66	219	60,89	305	145		81	9	
		0,0473	-16,37	421,5	263,39	159	-69		90	0	
		0,0302	-20,26	316,5	158,39	153	-63		77	13	
		0,0296	-20,44	237	78,89	131	-41		78	12	
2	1.0e-04	0,4063	0,00	156,5	156,74	329	121	121,92	78	12	2,44
		0,0444	-19,23	479	322,26	142	-52		79	11	
3	1.0e-04	0,3654	0,00	155	154,06	328	122	122,88	84	6	2,48
		0,0525	-16,85	226	71,94	143	-53		79	11	
4	1.0e-04	0,2441	0,00	152	152,12	324	126	126,66	84	6	2,51
		0,0629	-11,78	335	182,88	148	-58		90	0	
		0,039	-15,93	229	76,88	147	-57		90	0	
		0,0328	-17,43	266	113,88	163	-73		67	23	
5	1.0e-04	0,4553	0,00	150	149,94	326	124	124,52	80	10	2,55
		0,0349	-22,31	338,5	188,56	159	-69		84	6	
		0,0335	-22,67	329	179,06	198	-108		58	32	
6	1.0e-04	0,3111	0	147,5	147,45	318	132	131,74	76	14	2,59
		0,0506	-15,77	342,5	195,05	158	-68		77	13	
		0,0423	-17,33	162,5	15,05	92	-2		80	10	
		0,0387	-18,10	305,5	158,05	52	38		54	36	
7	1.0e-04	0,3598	0,00	145	145,45	319	131	130,34	87	3	2,63
		0,077	-13,39	341	195,55	192	-102		70	20	
		0,0498	-17,18	346,5	201,05	158	-68		86	4	
		0,0396	-19,17	191	45,55	91	-1		38	52	
8	1.0e-04	0,3875	0,00	143	143,26	317	133	133,44	89	1	2,67
		0,0799	-13,71	346,5	203,24	195	-105		80	10	
		0,0556	-16,86	350	206,74	143	-53		66	24	
		0,0481	-18,12	181	37,74	1	89		24	66	
9	1.0e-04	0,1296	0,00	147,5	0	316	134		90	0	
		0,0963	-2,58	349	201,5	197	-107		78	12	
		0,0467	-8,87	186	38,5	140	-50		80	10	
		0,0393	-10,36	165,5	18	196	-106		59	31	
		0,035	-11,37	314	166,5	145	-55		87	3	
		0,0316	-12,26	236	88,5	352	98		66	24	
		0,031	-12,42	328	180,5	145	-55		89	1	
		0,0296	-12,83	348,5	201	195	-105		56	34	
		0,0265	-13,79	289	141,5	92	-2		79	11	
		0,0267	-13,72	178	30,5	92	-2		79	11	
		0,0257	-14,05	188,5	41	92	-2		79	11	
		0,0259	-13,99	332	184,5	130	-40		59	31	
		0,0248	-14,36	396	248,5	322	128		76	14	
		0,0257	-14,05	354,5	207	322	128		76	14	
10	1.0e-05	0,6025	0,00	152	0	304	146		72	18	
		0,4292	-2,95	183	31	157	-67		71	19	
		0,3293	-5,25	309	157	158	-68		67	23	
		0,3009	-6,03	168	16	158	-68		59	31	
		0,2936	-6,24	420	268	353	97		70	20	
		0,2864	-6,46	305	153	158	-68		67	23	
		0,3101	-5,77	173,5	21,5	158	-68		67	23	
		0,2985	-6,10	180	28	158	-68		67	23	
		0,2802	-6,65	323,5	171,5	158	-68		59	31	
		0,2779	-6,72	177	25	158	-68		67	23	
		0,2608	-7,27	181,5	29,5	158	-68		67	23	
		0,2668	-7,08	186,5	34,5	158	-68		67	23	
		0,2404	-7,98	449	297	158	-68		67	23	
		0,2423	-7,91	330,5	178,5	158	-68		67	23	
		0,231	-8,33	314	162	158	-68		67	23	
		0,2225	-8,65	311,5	159,5	158	-68		67	23	
		0,2268	-8,49	190	38	158	-68		67	23	
		0,225	-8,56	417,5	265,5	127	-37		76	14	
		0,2276	-8,46	283,5	131,5	127	-37		76	14	
		0,2245	-8,57	285	133	60	30		74	16	
		0,2245	-8,57	266	114	158	-68		67	23	
		0,2252	-8,55	325,5	173,5	158	-68		67	23	
		0,2225	-8,65	349,5	197,5	158	-68		67	23	
		0,2258	-8,52	320	168	158	-68		67	23	
11	1.0e-05	0,6375	0,00	177,5	0	221	-131		80	10	
		0,5067	-1,99	420,5	243	349	101		84	6	
		0,3485	-5,25	279	101,5	52	38		83	7	
		0,3265	-5,81	299	121,5	52	38		83	7	
		0,3136	-6,16	302	124,5	73	17		69	21	
		0,2914	-6,80	319	141,5	139	-49		70	20	
		0,3022	-6,48	283,5	106	41	49		90	0	
		0,2465	-8,25	285	107,5	47	43		84	6	
		0,2398	-8,49	281	103,5	47	43		85	5	
		0,2384	-8,54	293	115,5	57	33		66	24	
12	1.0e-04	0,2502	18,39	182	20,5	220	-130		84	6	
		0,038	2,02	422,5	261	339	111		90	0	
		0,0336	0,96	275,5	114	34	56		75	15	
		0,0301	0,00	296	134,5	72	18		54	36	
		0,0294	-0,20	450,5	289	192	-102		75	15	
		0,0301	0,00	161,5	0	214	-124		35	55	

13	1.0e-04	0,2004	0,00	186	0	221	-131		86	4	
		0,0523	-11,67	275	89	39	51		75	15	
		0,0432	-13,33	312	126	139	-49		83	7	
		0,0391	-14,19	276,5	90,5	39	51		75	15	
		0,0362	-14,86	423,5	237,5	340	110		81	9	
		0,037	-14,67	271,5	85,5	39	51		75	15	
		0,032	-15,93	277,5	91,5	39	51		75	15	
		0,032	-15,93	279	93	39	51		75	15	
14	1.0e-05	0,471	6,10	190	16,5	230	-140		90	0	
		0,3163	2,64	267,5	94	27	63		88	2	
		0,2923	1,96	286,5	113	47	43		74	16	
		0,2717	1,32	293	119,5	47	43		74	16	
		0,2547	0,76	309,5	136	141	-51		81	9	
		0,2333	0,00	173,5	0	291	159		87	3	
		0,2287	-0,17	274	100,5	291	159		87	3	
		0,2318	-0,06	454,5	281	204	-114		77	13	
		0,2156	-0,69	175	1,5	291	159		88	2	
		0,2108	-0,88	271,5	98	348	102		52	38	
		0,2186	-0,57	426	252,5	348	102		52	38	
		0,2094	-0,94	201	27,5	322	128		71	19	
		0,2107	-0,89	522	348,5	348	102		52	38	
		0,2087	-0,97	289	115,5	47	43		72	18	
		0,1967	-1,48	249	75,5	322	128		71	19	
		0,1909	-1,74	254,5	81	87	3		71	19	
		0,1891	-1,82	310	136,5	322	128		71	19	
		0,1823	-2,14	305	131,5	194	-104		46	44	
		0,1856	-1,99	244	70,5	322	128		71	19	
		0,1801	-2,25	320,5	147	225	-135		71	19	
		0,1766	-2,42	340	166,5	335	115		80	10	
		0,1794	-2,28	241,5	68	322	128		71	19	
15	1.0e-05	0,4712	4,94	194,5	15,5	240	-150		88	2	
		0,5396	6,12	289	110	47	43		88	2	
		0,4308	4,16	283,5	104,5	45	45		77	13	
		0,3504	2,37	286	107	46	44		84	6	
		0,3016	1,06	454,5	275,5	348	102		63	27	
		0,3134	1,40	254,5	75,5	348	102		63	27	
		0,3194	1,56	275,5	96,5	46	44		84	6	
		0,2762	0,30	280,5	101,5	46	44		84	6	
		0,2739	0,23	243,5	64,5	348	102		63	27	
		0,2685	0,06	250	71	348	102		63	27	
		0,2611	-0,19	458	279	348	102		64	26	
		0,2644	-0,08	267,5	88,5	345	105		64	26	
		0,2561	-0,36	271,5	92,5	345	105		64	26	
		0,2668	0,00	179	0	345	105		86	4	
		0,2281	-1,36	252	73	289	161		64	26	
		0,2356	-1,08	260	81	345	105		64	26	
		0,2228	-1,57	342,5	163,5	345	105		77	13	
		0,2265	-1,42	522,5	343,5	329	121		77	13	
		0,2049	-2,29	245,5	66,5	329	121		77	13	
		0,1991	-2,54	456,5	277,5	329	121		77	13	
		0,2039	-2,34	427	248	329	121		78	12	
		0,2161	-1,83	430	251	329	121		78	12	
		0,2104	-2,06	240	61	329	121		78	12	
		0,2033	-2,36	266	87	329	121		78	12	